2005

Confocal Laser Scanning Microscopy As A Tool For The Investigation Of Tetracycline Fluorescence In Archaeologicalhuman Bone

Corey Maggiano
University of Central Florida, cmaggian@westga.edu

CONFOCAL LASER SCANNING MICROSCOPY AS A TOOL FOR THE INVESTIGATION OF TETRACYCLINE FLUORESCENCE IN ARCHAEOLOGICAL HUMAN BONE

by

COREY M. MAGGIANO
B.A. University of Central Florida, 2002

A thesis submitted in partial fulfillment of the requirements
for the degree of Master of Science
in the Department of Biology
in the College of Arts and Sciences
at the University of Central Florida
Orlando, Florida

Fall Term
2005

Confocal Laser Scanning Microscopy as a Tool for the Investigation of Tetracycline Labels in Archaeological Human Bone

In Holdings at the University of Central Florida Library
Orlando Florida 32816

ABSTRACT

Fluorochromes such as tetracycline have been used to label bone for histomorphometric analysis, measuring bone formation, growth, maintenance, and pathology. More recently, similar fluorescence has been observed in ancient human bone. Attributed to tetracycline (TC) exposure, this phenomenon could affect various aspects of health during life and/or preservation of remains postmortem. Standard epifluorescence microscopy is the most common tool employed in the analysis of these labels. Though valuable, this technique is limited by its inability to penetrate bone three-dimensionally and its inclusion of out-of-focus light, possibly disrupting accurate analysis. Confocal Laser Scanning Microscopy (CLSM) has been demonstrated as a valuable tool for three-dimensional histology. Its application to the study of compact bone fluorescence has been lacking, especially in archaeological and forensic sciences. In the following two papers, modern TC-controlled bone is compared to well preserved archaeological bone recovered from the Dakhleh Oasis, Egypt, using both standard wide-field and more modern confocal techniques for imaging and analysis. Spectral analysis via CLSM shows that both modern and ancient fluorescent labels in bone share the exact same fluorescence emission peak at 525 nm. Differences in the shape of the spectral curve and photobleaching characteristics are discussed. In addition, CLSM's high-resolution two- and three-dimensional imaging capabilities (in polarized light, scattered light, and fluorescence light) are found to increase the flexibility and creativity of investigations into the occurrence of tetracycline labels in archaeological bone and could have added benefits for modern medical and anatomical experimentation.

To My Loving Family

and

Devoted Followers of

Subpolymorphicnontrilinearsemiduelistichyperatypicalantipostpseudorecatagoriz-

ationalisticalitarianism

ACKNOWLEDGMENTS

Most importantly I would like to thank my family and friends for their tolerance and encouragement and the members of my committee for their patience and flexibility: Jane Waterman, Tosha Dupras, John Schultz, Robert Shetlar, John Biggerstaff, and Michael Schultz. It is not often that multidisciplinary work receives such open-minded and well-informed support from members of each of the contributing fields, and for that I am grateful. I would also like to thank D.C. White and members of the Biomarker Research Facility of the University of Tennessee, Knoxville, including M. Le Puil and B. Weidow from the Biological Imaging Unit as well as J. Dunlap for his generous guidance on CLSM systems and D. Gerard and R. Smith at the University of Tennessee for control sample contributions. In addition, I am indebted to C. Viebahn and members of the Paleopathological Research Facility at the Zentrum Anatomie, Georg-August-Universität, Göttingen, Germany, including M. Brandt, I. Wanner, N. Roumelis, J. Novacek, and S. Flohr for their guidance in sample preparation, histology, and microscopy techniques, as well as M. Rupnik from the European Institute for Neurobiology. I am also thankful for the cooperation of the Egyptian Supreme Council of Antiquities and members of the Dakhleh Oasis Project, in particular: A. J. Mills, J. E. Molto, P. Sheldrick, M. Tocheri, C. A. Hope, G. E. Bowen, U. Thanheiser, and C. Churcher. This research was conducted at the Biology Department of the University of Central Florida and supported by grants from The Wenner-Gren Foundation for Anthropological Research and In-House Grants from the University of Central Florida Graduate Studies Department and Student Government.

TABLE OF CONTENTS

LIST OF FIGURES

LIST OF TABLES

CHAPTER 1

GENERAL INTRODUCTION

Originally, the intent of my investigations into ancient antibiotics and tetracycline labeling of bone was to reopen a line of studies begun in the 1980's by Basset, Armelagos, Keith, Cook and several others (Bassett et al. 1980; Keith and Armelagos 1983, 1988; Cook et al. 1989). They discovered yellow-green fluorescent labels in human bone over a thousand years old, morphologically identical to those created during modern medical administration of tetracycline (TC). Exposure TC could have affected populations' health in various ways, including resistance to bacterial infection, bone degenerative processes, and disfigurement of fetal hard tissues. Unfortunately, research on the subject has been scarce since this time period.

Therefore, I designed a pilot project to test the skeletal samples from the Dakhleh Oasis, Egypt, providing evidence from a different region and time period. Because bacterially infested grain products are the suggested source for TC consumption, I tested animal bone from the same area. Fetal bone was also examined due to the transference of TC via placenta. A more modern confocal laser scanning microscopy was used for fluorescence imaging of the bone. Results of these pilot projects supported the findings of previous researchers (Maggiano et al. 2003). Not only was the fluorescent substance morphologically similar to TC incorporated into human bone but it was also present in fetal and animal remains as well.

Immediately the most important realization made was that in all cases of ancient antibiotic so far published, over 90% of all examined individuals showed evidence for TC exposure. The logical next step was to use population level analysis and demographics correlations to determine: 1) who was most affected, 2) what health effects were probable, and 3) what the most likely mechanism was for exposure. Although previous researchers had attempted something similar, problems arose when others noted that natural processes of decomposition and postmortem bacterial infestation could account for fluorescence in bone (Piepenbrink 1983).

Therefore, I decided that instead of rushing to achieve population level analysis, perhaps it was better to learn more about the specifics of ancient tetracycline fluorescence. Along the way I wanted to collect support for the use of CLSM as a tool by which further investigation could discern the difference between 2000 year old Roman-Egyptians on antibiotic regimens and microscopic fluorescence artifacts from soil bacteria. In the process I found that CLSM may have benefits for general histomorphometric analysis in bone and could offer new three-dimensional perspectives to the structure of bone microarchitecture. The first two steps of this process were to examine the use of CLSM for spectral analysis of fluorescent substances within bone and to demonstrate its capabilities for fluorescence, polarized light, and three-dimensional imaging of bone histology in general. Therefore, the following two chapters detail the use of Confocal Laser Scanning Microscopy for spectral and image analysis of ancient tetracycline labels found in Roman-Egyptian human bone dating to roughly AD 100-400.

References

Armelagos GJ. 2000. Take two beers and call me in 1,600 years. Natural History 109(4): 50-4.

Bassett E, Keith M, Armelagos GJ, Martin D, and Villanueva A. 1980. Tetracycline-labeled human bone from ancient Sudanese Nubia (A.D. 350). Science 209: 1532 -4.

Cook M, Molto E, and Anderson C. 1989. Fluorochrome labelling in Roman period skeletons from Dakhleh Oasis, Egypt. American Journal of Physical Anthropology 80(2):137-43.

Keith M and Armelagos GJ. 1983. Naturally occurring antibiotics and human health. In: Romanuuci L, Moerman D, and Tancredi L, editors. The Anthropology of Medicine. New York: Bergin and Garvey Publishers pp.68-79.

Keith M and Armelagos GJ. 1988. An example of in vivo tetracycline labeling: Reply to Piepenbrink. Journal of Archaeological Science 15:595-601.

Maggiano C, Dupras T, and Biggerstaff J. 2003. Ancient antibiotics: evidence for tetracycline in human and animal bone from kellis. In: Mills AJ and Hope CA, editors. The Dakhleh Oasis Monograph. vol.3. Oxford: Oxbow Books pp.331-344.

Piepenbrink H, Herrmann B, and Hoffman P. 1983. Tetracylintypische fluoreszenzen and bodengelagerten skeletteilen. Zeitschrift fur Rechtsmedizin 91:71-4.

CHAPTER 2

SPECTRAL AND PHOTOBLEACHING ANALYSIS USING CONFOCAL LASER SCANNING MICROSCOPY: A COMPARISON OF MODERN AND ARCHAEOLOGICAL BONE FLUORESCENCE

Introduction

Natural fluorescence of bone in response to ultraviolet to blue (UV-B) wavelength light is due to collagen autofluorescence, providing relatively faint, diffuse light, depending on the thickness of the sample observed. However, Milch, Rall, and Tobie (1957, 1958) observed localized, bright, yellow-green fluorescence in microscopic bone structures formed during tetracycline administration. Frost, Villanueva, and many others (Frost et al. 1961; Rush et al. 1966; Taylor and Frost 1966; Villanueva et al. 1983) used TC labeling and staining techniques to provide microfluorescence analysis of bone, measuring rates of bone growth between fluorescent "labels" and locating mineralization fronts. These efforts have contributed greatly to the understanding of bone diseases and normal bone growth, healing, and adaptive response. Fluorescent labels in bone could have implications for archaeological and forensic sciences as well.

The histology of thin ground bone sections is an integral part of archaeological investigation into the health of ancient peoples. Despite their age, archaeological bone maintains its microscopic architecture, in some cases for tens of thousands, even millions

of years (Stout and Teitelbaum 1976; Stout 1978; Schultz 2001). In 1980, Basset and colleagues (Bassett et al. 1980, Keith and Armelagos 1983) were the first to report tetracycline-like fluorescence in archaeological human bone recovered from a site in Sudanese Nubia (circa AD 350). They noted the most likely source for TC exposure was through the consumption of bacterially contaminated grain or ale (Armelagos 2000). Subsequently, similar bone fluorescence has been documented at ‘Ain Tirghi (Cook et al. 1989) and the Kellis cemeteries of the Dakhleh Oasis, Egypt (Maggiano et al. 2003), supporting a local continuance of the phenomenon for over 1200 years. Drastic health affects are possible in response to ingested TC, but reports disagree in the likelihood of therapeutic-blood concentrations in ancient times. In addition to their antibiotic effects, TC and its isomers also inhibit bone degenerative diseases and cancerous growth (Gilbertson-Beadling 1995; Sadowski and Steinmeyer 2001) and can cause staining, growth interruption, and even disfigurement of forming hard tissues (Urist and Ibsen 1963; Saxen 1966; Johnson and Mitchell 1966). Placental and lactate transference of TC renders infants especially vulnerable to TC’s negative side effects (Skinner and Nalbandian 1975), prompting the recommendation that pregnant and nursing women avoid TC drug treatments (Walsh 2000).

In vivo, TC labels form due to natural fluorescence and chemical affinities for hard tissues (Misra 1991). Bone is a composite material comprised of two main structural elements: the mineral, hydroxyapatite, which lends bone its strength; and the organic, primarily collagen (type I), for flexibility (White 2000). Formation, maturation, and maintenance of bone proceeds via localized cycles of bone resorption and appositional calcification of bone cell secretions. In humans, periosteal growth results in

layers of lamellar bone running the whole or part of the circumference of a long bone. With maturation, however, the base structural unit of compact bone becomes the osteon (Eriksen et al. 1994), or Haversian system, a layered cylindrical tube surrounding bone vascular tissue (Figure 1).

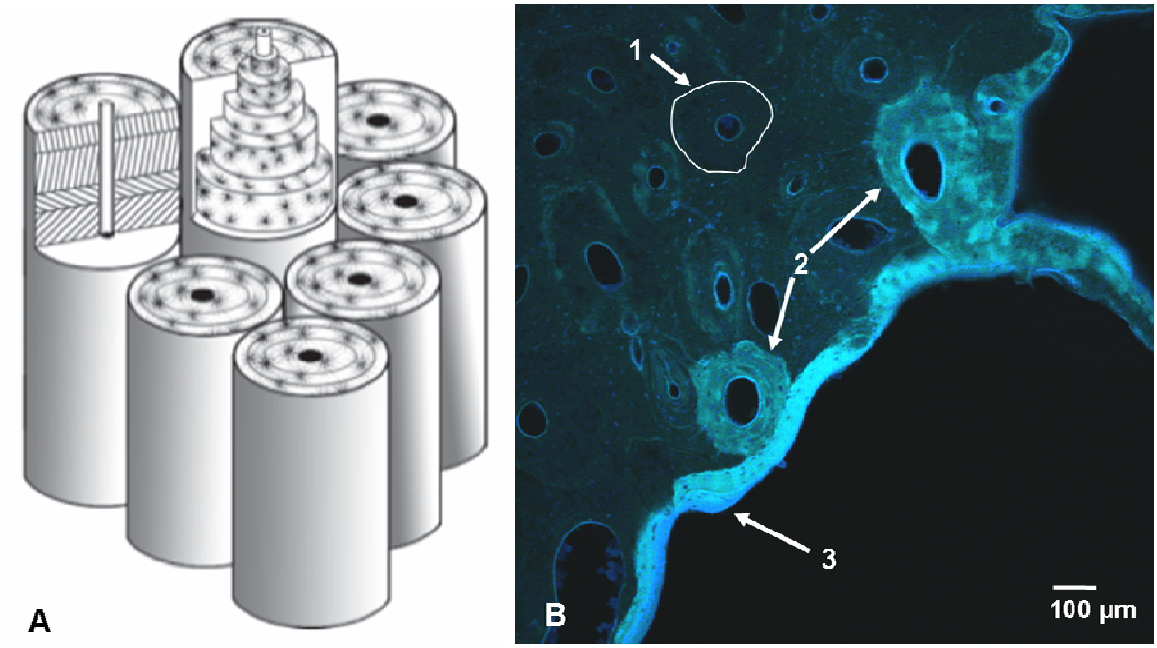

Figure 1.1: Basic Microstructure of Mature Cortical Bone. A) Cylindrical representations of layered Haversian systems, or osteons (courtesy of L. Williams). B) Two-dimensional confocal laser scanning microscopic image of archaeological bone fluorescence from individual D7-8, from the Kellis town site, Dakhleh Oasis, Egypt, showing: 1) non-fluorescent osteon (white perimeter hand-drawn for clarification), 2) two completely fluorescent osteons, and 3) fluorescently labeled internal circumferential lamellae. Scale notes 100µm at 100x total magnification.

When viewed in cross section these structures appear "bulls-eye-like", with a canal in the center. Networks of osteons are responsible for the structural integrity and nutrient supply of mature human compact bone (Burr et al. 1998). Differences in bone histomorphometry can be significant between mammal species and between individuals of differing ages, but the chemical and physical process of TC label formation remains similar.

Tetracycline, ingested or injected in sufficient doses pervades all body tissues, including bone, via the bloodstream (Van der Bijl and Pitigoi-Aron 1995). Due to hydrogen bonding and other weak chemical forces, TC molecules settle within the calcium-phosphate crystalline lattice of hydroxyapatite (Nielsen and Gyrd-Hansen 1996; Misra 1991). This diffuse labeling is temporary and is lost to excretion within about three days unless new bone is being formed in that region (Frost 1965). In areas of calcification, however, TC molecules are locked between apposing layers of bone. A single exposure creates a thin band in lamellar bone, or a ring in an osteon. Repeated exposures over time can result in the labeling of the entire structure (Cook et al. 1989). Six morphological forms of fluorescence have been identified in archaeological bone, based on the structures labeled and suspected exposure durations, including "ring", "complete", and "lamellar" labels (Maggiano et al. 2003). *In vivo,* labels enduring for years will eventually be reabsorbed into the bloodstream. Postmortem, labels fade depending on pH and light exposure; locked within bone, they can persist for many years (Frost 1965).

Fluorescent labels in bone, whether modern or archaeological, are most commonly observed using epifluorescence microscopy. This technique uses a high-powered illumination source, normally a halogen or mercury arch lamp, to excite the fluorochrome. A dichroic filter separates the emitted fluorescent light from the incident light, allowing the collection of certain fluorescence wavelengths. To change the wavelengths of collected light, filters must be exchanged manually. Like other wide-field microscopic systems, inclusion of out-of-focus light from above and below the focal plane clutters the field of view with fluorescent "noise", diminishing achievable

resolution and confusing label analysis due to overlapping and obscured structures (Birkenhäger-Frenkel and Birkenhäger 1987). This means samples must be made extremely thin, decreasing the volume of observable tissue and adding to the labor involved in sample preparation, especially when working with hard materials such as undecalcified bone. Full spectral analysis of fluorochrome labels is not possible without additional equipment.

Spectral characteristics of fluorescence: emission peak, maximum intensity, and fluorescence range, are specific both to the chemical structure of the fluorochrome(s) and its relative concentration within the observed sample (in three dimensions). Under controlled lab conditions, TC concentrations in aqueous solution can be determined by analysis of fluorescence intensity (Horvath and Glazier 1993). Standard microscopic techniques do not permit simultaneous image analysis and comparison of spectral data from specific regions of interest within or between fields of view.

Eliminating many of the limitations of epifluorescence microscopy, modern confocal laser scanning microscopy (CLSM), provides greater z-axis resolution, simultaneous multi-wavelength fluorescence imaging, and 3-D reconstruction of tissues over 100 μm in thickness (Biggerstaff et al. 1997, 1998; Boyde et al. 1994). Confocal microscopes use a system of intense, finely focused lasers (~0.2 μm in diameter) for incident illumination. A computerized operating system manipulates mirrors, rapidly scanning the laser across the focal plane and inducing excitation in the target fluorochrome(s). Diffuse out-of-focus fluorescence from above and below the focal plane, is refocused either before or after an adjustable pinhole. Thus, only light from the focal plane passes through the pinhole. The focal plane can be moved up or down within

the sample to generate 3-D stacks or to view any depth without the influence of out-of-focus light. An electronically controlled crystalline filter, called an acousto-optical tunable filter (AOTF), permits only light at chosen wavelengths to reach the photon detector(s). The computer correlates photon impacts with the laser's scanning position and to create a digital image of fluorescence in the sample.

The only major limitation of CLSM for postmortem analysis of tissues is that, due to the strength of the light source and z-axis excitation depth, continued scanning induces fading in the fluorescence signal, or photobleaching (Cahalan et al. 2002). This is caused by chemical modification of the fluorochrome due to repeated excitation/emission states. However, spectral detection and/or larger volume three-dimensional image reconstruction may require longer scanning times. Consequently, the photobleaching effect could be more significant. The rate at which a sample looses its fluorescence is determined by the amount of fluorochrome present, the intensity of the incident light, the refractive index of the medium or target, and the photochemical properties of the molecule itself; in some cases complete bleaching occurs in just seconds (Song 1997; Van Oostveldt et al. 1998). For our analysis, faded emission is unrecoverable and should be avoided. Therefore, it is necessary to identify the photobleaching rate and the function of emission decay in order to avoid or correct for this phenomenon (Ono et al. 2001).

Recent advances in CLSM technology permit real time, three-dimensional, spectral analysis of fluorescent material. Despite its benefits, the use of CLSM for imaging in modern histomorphometric analysis of bone is only now gaining popularity and its application to archaeological investigation is rare. The current study employed confocal laser scanning microscopy for *in situ* spectral analysis, quantifiably comparing

tetracycline fluorescence of modern and archaeological bone. In addition, photobleaching tests were performed in order measure the decrease in fluorescent intensity over time for future CLSM bone analyses. Three types of bone tissue were tested: 1) modern pig alveolar bone from individuals double-labeled with tetracycline via injection; 2) archaeological human humeral bone from the Dakhleh Oasis, Egypt (circa AD 100-400), and 3) a stained, decalcified dog femur. We hypothesized that CLSM would provide an accurate means for spectral characterization and intensity measurement, compared with expected values from the literature. Our preliminary CLSM experimentation also leads to the hypothesis that photobleaching effects are not problematic for standard two- and three-dimensional scanning.

Materials and Methods

Sample collection and processing

The archaeological sample was recovered by the Dakhleh Oasis Project under the directorship of Anthony Mills. Selected individuals are from the Kellis 2 cemetery and associated Kellis town site of the Dakhleh Oasis, Egypt, dating to approximately AD 100-400 (Hope 2001; Molto 2001). Studies from archaeological sites in the Sudan and Egypt report that nearly every tested individual displays some evidence of TC fluorescence (Basset et al. 1980; Keith and Armelagos 1983; Cook et al. 1989; Armelagos 2000; Maggiano et al. 2003). Therefore no examination of individuals was necessary to predict the occurrence of fluorescent labeling prior to experimentation. For the current study, four individuals were examined, B400, B427, B443, and D7-8.

Transverse cross sections were removed from these adult skeletons during sampling for DNA and stable-isotope analysis at the mid-diaphysis of the left humerus. This location was considered ideal for its thick cortical bone and remoteness from areas important for estimations of age or sex.

Previous studies have shown that autofluorescence of the label and the tissue itself is sufficient for CLSM imaging with no additional treatments or probes necessary (Maggiano et al. 2003). Thin-ground sectioning was performed on the undecalcified archaeological bone as described by Schultz (Schultz 1988, 2001). Samples were plastinated using the Biodur® preparation technique. Reportedly, this technique offers optimum penetration of micro-porous structures and seamless joining with internal and external surfaces, eliminating artifacts that sometimes arise from faster curing epoxy resins and prologing the "lifetime" of the sample. Slides produced were measured by micrometer at ~70 μm and cover-slipped. Drawings were made from a magnifying projector and key features were micro-photographed using Hilfsobject red quartz compensator enhanced polarization.

All samples were analyzed for pathology and diagenesis at the Zentrum Anatomie, Georg-August-Universität, Göttingen, Germany. Slides selected for this study were negative for obvious metabolic, degenerative, or infectious disease and demonstrated excellent preservation with no signs of generalized chemical or biological destruction. Original internal and external surfaces were intact and postmortem fragmentation and micro-fractures were absent. Localized artifacts of diagenesis in ancient bone are unavoidable, but polarized light microscopy revealed that samples

contained well-organized collagen content, demonstrating that even the organic components of the bone were generally unaffected.

Two modern sections from pig alveolar bone were used as positive controls for TC fluorescence. These samples were prepared using standardized methods for histomorphometric investigation using TC double labeling (Carr et al. 1996a, 1996b). Pigs had been given two premortem doses of TC. Thin-sectioned decalcified dog bone was also obtained. These had been stained with hematoxylin and eosin, embedded in paraffin, and thin sectioned to 20 μm via microtome. Both eosin stain and collagen are fluorescent under UV-B excitation. However, since no mineral component remains for TC chelation (Fukutani et al. 1985), these samples serve as negative controls for tetracycline fluorescence.

Microscopic detection and spectral analysis

Fluorescence analysis was achieved using three techniques: 1) spectral analysis, which measures emitted light intensities at intervals of 7 nm across the total spectrum, generating curves via intensity profiles; 2) intensity comparison, demonstrating the difference in intensity between different structures within a sample; and 3) photobleaching tests, showing the decline in fluorescent intensity over time resulting from chemical alteration of the fluorochrome.

A Leica SP2 confocal microscope with an argon ion laser light source was used for all fluorescence analysis. Beam splitters ensured that the 458 nm laser line was used for excitation. Due to its weakness in comparison with the natural line at 488nm, relatively high laser power was used (100% software setting, 25% manual) except during

photobleaching tests. The excitation peak for TC is wide but roughly peaks around 390 nm (Hoerman 1975). Studies using CLSM have shown that laser excitation at 458 nm induces ample excitation of modern and ancient fluorescence in bone (Maggiano et al. 2003; Boyde et al. 1994). During scanning, fields of interest were preferred that contained both ring fluorescence and thicker labels, such as complete osteon fluorescence in the archaeological samples. The "over/under" LUT (contrast stretching) option ensured system settings were not used to distort the dominance of features through over or under exposure (detector saturation or non-detection). Imaging parameters such as objective, beam splitter, laser power, pinhole size, PMT sensitivity, z-position, pixel dimensions, emission detection range, and the number of scans were recorded for each image.

Spectral analysis settings were standardized for all samples, notably: 10x 0.3 NA objective, 256 pixel resolution, 599 V PMT, and pinholes at 84.89 μm and 1.00 airy. The focus was adjusted each time to reach the maximum plane of fluorescence (at an emitted range 500-600nm). During each scan, the RD 70/30 intensity reduction mirror was used, permitting detection of the full range of emitted light. Although the TD 488/543/633 triple-dichroic mirror allows better image quality due to greater emission intensities, it filters out a large portion of the TC emission range from 520 nm to 570 nm. This creates an artificially double-peaked spectrum and is therefore not suitable for spectral scanning of these fluorochromes. The AOTF collected a range of emission 7 nm wide that was moved down-spectrum in 7 nm steps for each scan (35 scans total, from 471 nm to 708 nm). The process was repeated for each sample or field of view examined.

Preliminary observations suggested modern samples had only slight variation in label intensity between individuals (14). This was expected due to the mechanics of label incorporation and standardization of lab techniques involved in TC double labeling. Therefore, for positive controls three different fields of view were chosen from pig BR3-4#1. Archaeological labels, however, have obviously variable intensities and therefore three different individuals (B427, B443, and D7-8) were sampled for fluorescence on the chances that the spectra were likewise variable. In most archaeological fields of view, ring fluorescence was not bright enough for spectral analysis so thicker labels were chosen (complete osteon or circumferential lamellar labels).

After the images were collected, regions of interest (ROI) were chosen for each field of view and replicated in each of the 35 images taken during spectral scanning. Three ROIs per field of view were selected to represent: 1) the fluorescent label, 2) the background fluorescence from bone not labeled with fluorochrome, and 3) the true baseline fluorescence from a region off the sample but in the same field of view. The morphological feature labeled with the highest intensity was selected to represent fluorescence within that field of view. Baseline values represented ROIs of only the slide, Biodur®, and cover slip. Often the vacant center of a porous cavity in the bone section was used for the baseline ROI. The mean intensity of pixels within each ROI was recorded per image, per sample. Intensity values were plotted against the wavelength of emission to produce spectral curves.

Designations were given to each ROI and resulting spectral curve as follows: decalcified dog bone fluorescence (ddFL), modern bone dentition with ROI on and off the fluorescent label (mdFL+ and mdFL- respectively), modern periosteal bone on and

off the fluorescent label (mpFL+ and mpFL- respectively), modern canal ring fluorescence on and off the label (mrFL+ and mrFL- respectively), archaeological complete osteon fluorescence, on and off the label (B427FL+ and B427FL- respectively), archaeological laminar bone fluorescence on and off the label (B443FL+ and B443FL-) respectively, and archaeological complete osteon fluorescence on and off the label (D7-8FL+ and D7-8FL- respectively). For all designations "FL = "fluorescent label" and "+/- " = "on/off" the label.

In addition, collected spectral scans from individual B443 were reanalyzed (not rescanned) to determine the variation in intensity between morphologically different sources of fluorescence. Ten ROIs were investigated on each of the two dominant fluorescent structures within the field of view: the internal lamina and an osteon. In this way ten spectra were generated for each morphological feature and the average spectra and average peak intensities of the two labels could be compared.

Fluorescence decay at standard scanning parameters

Photobleaching tests were performed on one modern (BR3-4#3) and one archaeological sample (B400) using each of the most common objectives for bone histomorphometric analysis: 10x, 20x, and 40x (NA = 0.3, 0.7, and 1.25 respectively). Photobleaching was accomplished by progressive scanning of images (N=2122) at 1.7 second intervals (400 Htz scan).

New fields of view were used for each photobleaching scan. Again, ROIs were the area of brightest fluorescence and the background fluorescence off-label (two ROIs per field of view). ROIs were designated modern or archaeological ("Mod" or "Arch")

for each objective used (10xMod, 10xArch, etc). The average pixel intensity within each ROI for each image was plotted against time. This was repeated for each set of experiments. Microscope settings were recorded and standardized for each magnification group, with the notable exception that the 10xMod test was run at lower PMT of 434.7 (all others were at 530.8). In order to speed up the bleaching process, a scanning zoom was used. The 40x experiments were run at 4x scanning zoom and all others used 5x scanning zoom. Results of photobleaching tests were standardized for intensity since the function and rate of photobleaching were the desired characteristics.

Results

CLSM spectral analysis

Results of CLSM spectral analysis showed baseline fluorescence on all samples is below ~10 on a scale of intensity (measured in arbitrary intensity units, or "AIU")

(Figure 2).

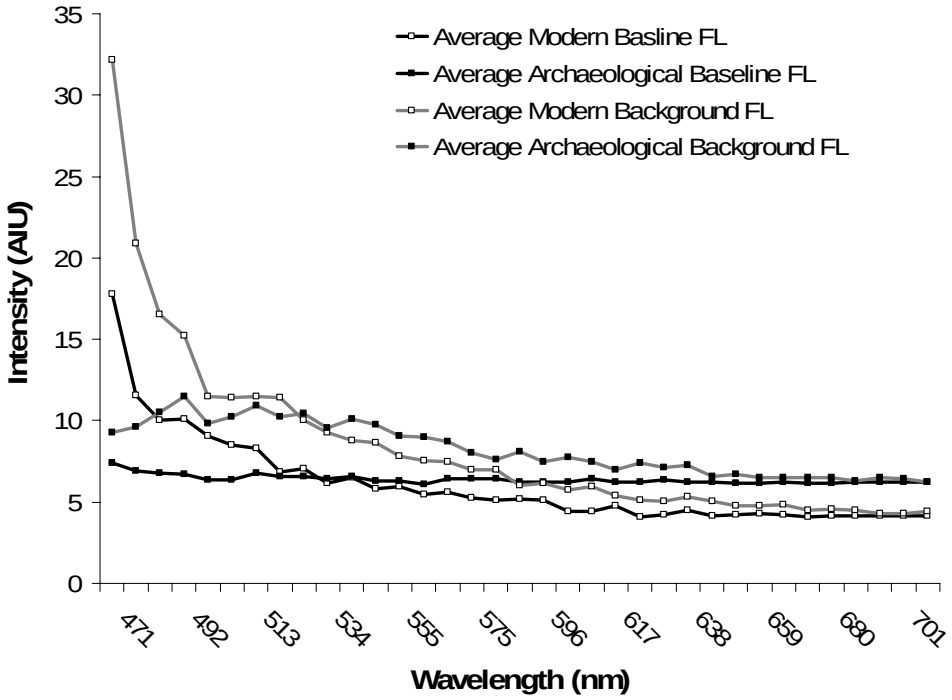

Figure 1.2: Confocal laser scanning microscopic spectral analysis of averaged baseline (black) and background (gray) fluorescence in modern (white-marked) and archaeological (black-marked) samples. Modern samples show greater intensity at wavelengths approaching excitation (458 nm). Intensity measured in arbitrary units, AIU.

The exception was that modern TC samples had higher intensity before 527 nm (25 AIU for mpBASE) dropping rapidly thereafter. Modern baseline fluorescence reached 33 AIU at 471 nm (as it approached the excitation wavelength). At higher wavelengths, modern non-label fluorescence decreased to two points lower than archaeological intensity. Archaeological samples displayed baseline intensities steady at 6-7 AIU across the spectrum and background fluorescence fluctuated from 6-11 AIU. No intensities below 3 AIU were reported for any measurement.

In response to 458 nm excitation, decalcified dog bone emission has a peak of 76 AIU at 562 nm (range 527-687 nm, 160 nm long) (Figure 1.3).

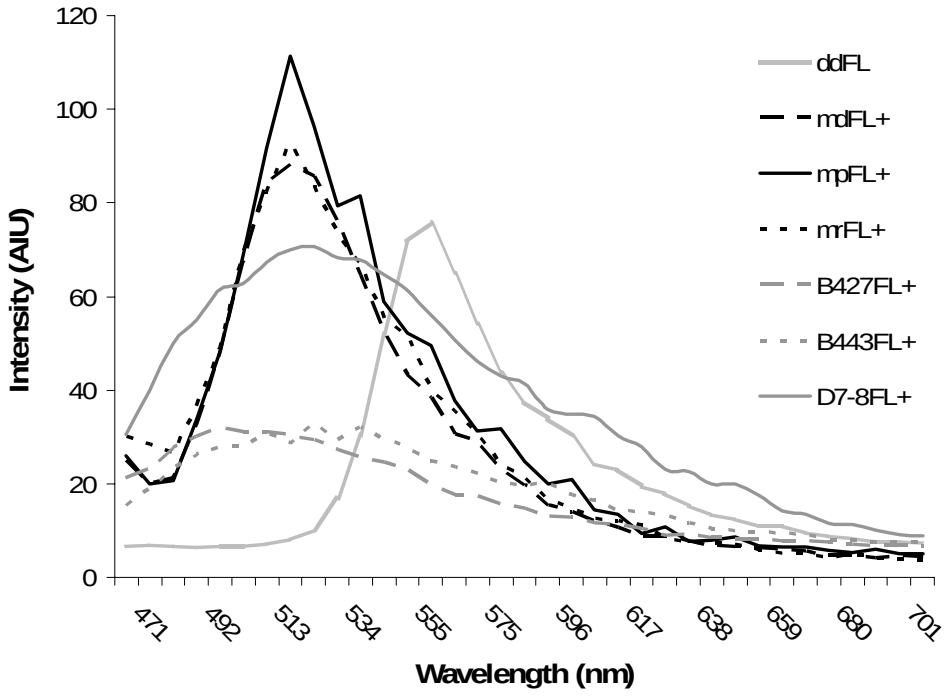

Figure 1.3: Confocal laser scanning microscopic spectral analysis of modern and archaeological bone fluorescence. During 458 nm laser excitation both modern (black solid, dashed, dotted) and archaeological TC labels (grey solid, dashed, dotted) have a fluorescence emission at 525 nm. Decalcified dog femur (light grey) stained with hematoxylin and eosin emits a single peak at 562 nm. Intensity measured in arbitrary units, AIU.

Modern TC ROIs (mdFL+, mpFL+, and mrFL+) emit sharp peaks of fluorescence of 88 to 111 AIU at 525 nm (range 478 – 678 nm, 200 nm long). Archaeological ROIs from the fluorescent label (B427FL+, B443FL+, and D7-8FL+) had lower and more variable averaged intensities (32 – 71 AIU). Spectra originating from archaeological samples have very gradual peaks 500 – 540 nm, but generally the common peak is ~525 nm. The range of archaeological spectra varies most drastically between D7-8 and B427

(84 nm difference at the yellow end of the spectrum). The average range for archaeological samples is from 471 – 665 nm, or 194 nm long.

Comparison between average intensity curves produced by laminar and complete osteonal fluorescence from a single field of view (individual B443) showed both resulting curves had peaks at ~525 nm (Figure 4). A z-test to compare intensity between the two means demonstrates a significant difference ($P = 0.039$) between the more intense fluorescence at the internal lamina (31 AIU maximum) and the completely labeled osteon (24 AIU maximum).

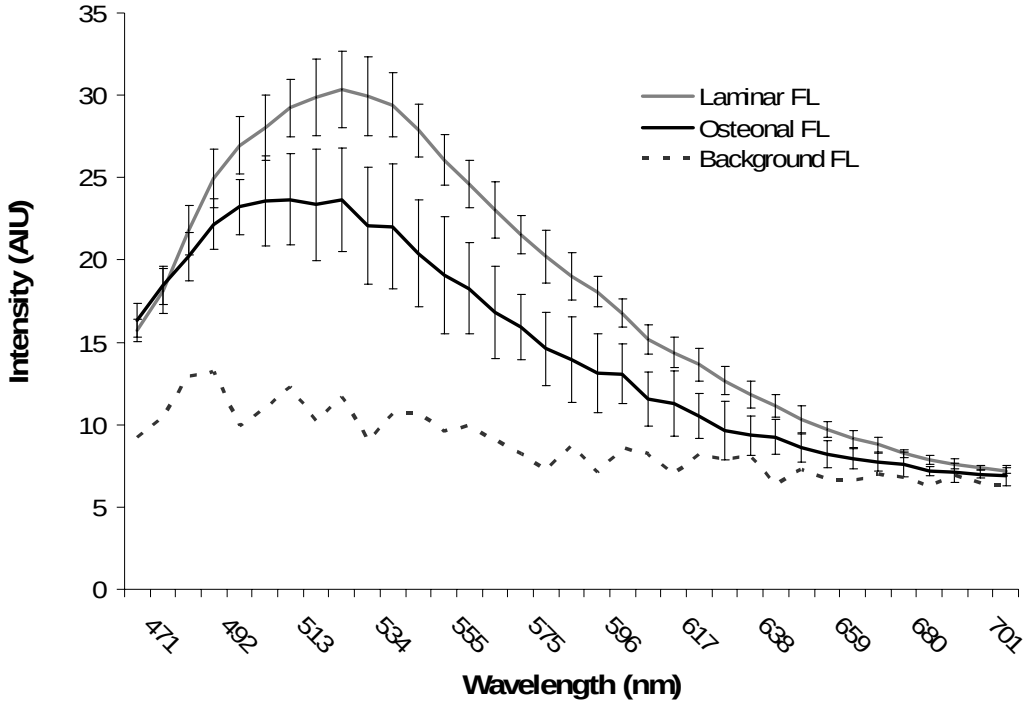

Figure 1.4: Compared average intensities from two fluorescent labels in individual B443 from the Kellis 2 cemetery of the Dakhleh Oasis, Egypt. The gray line denotes fluorescence from the internal lamina, or circumferencial lamella, while black marks that of an internal, completely fluorescent osteon. The dotted line notes background fluorescence off-label. Laminar fluorescence is significantly more intense, P = 0.039. Intensity measured in arbitrary units, AIU.

Photobleaching tests

After an hour of continuous scanning, a decrease in fluorescence intensity was detectable for all objectives (10x, 20x, and 40x) (Figures 5 and 6).

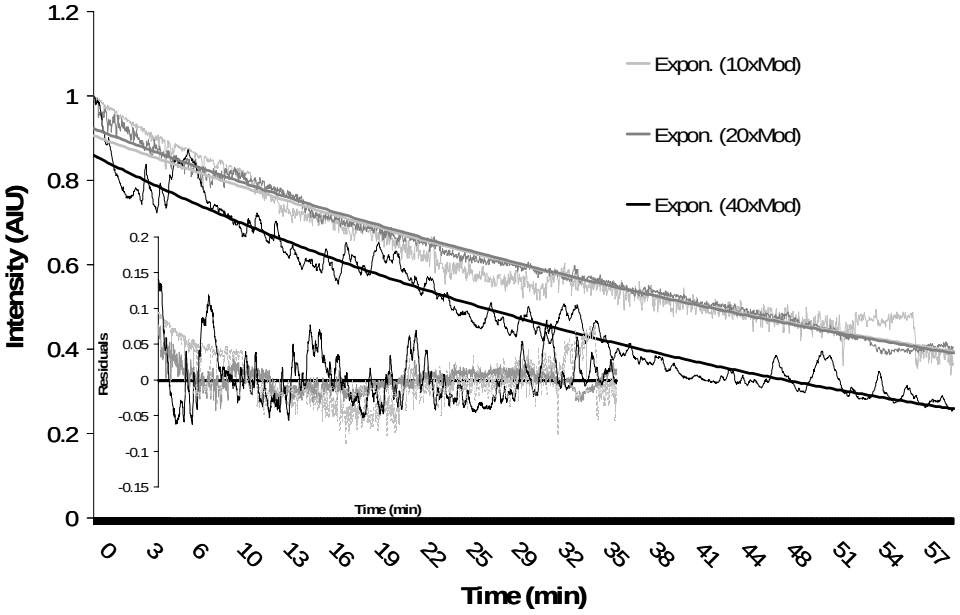

Figure 1.5: Photobleaching tests for modern TC controls. Smooth lines represent the exponential fit for intensity data collected using each objective (light grey, 10x = R^2 of 0.95, dark grey, 20x = R^2 of 0.99, and black, 40x = R^2 of 0.96 respectively). Inset shows that the distribution of residuals between experimental values and the fitted curve agree with a single-exponential function. Intensity is standardized. Total scanning-time was one hour.

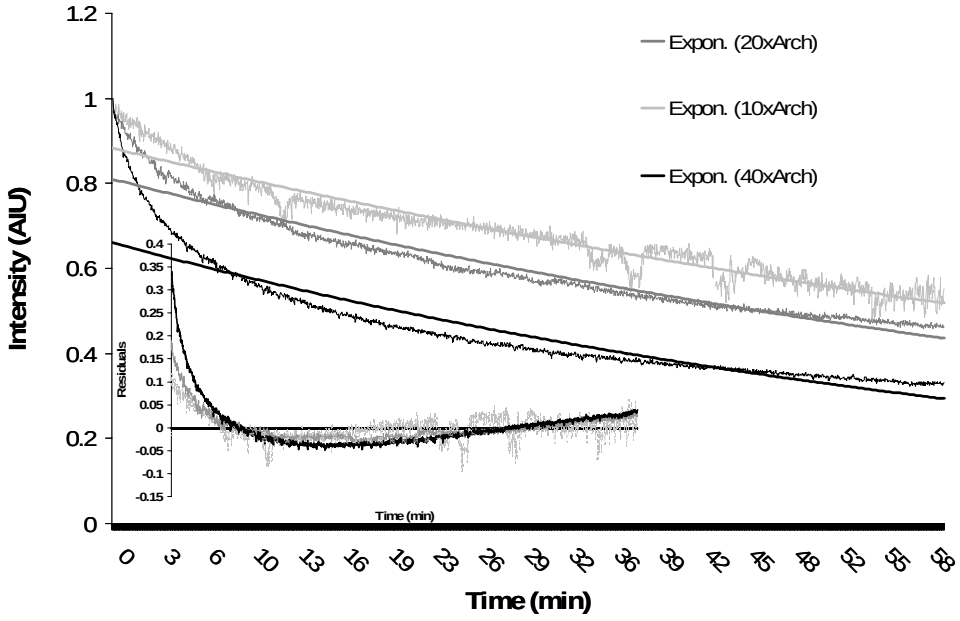

Figure 1.6: Photobleaching tests for archaeological fluorescence. Smooth lines represent the exponential fit for intensity data collected using each objective (light grey, 10x = R^2 of 0.95, dark grey, 20x = R^2 of 0.99, and black, 40x = R^2 of 0.96 respectively). Inset shows that the distribution of residuals between experimental values and the fitted curve notably deviates from a single-exponential function. Intensity is standardized. Total scanning-time was one hour.

Average background fluorescence decreased from 17 to 10 AIU by 20 min and never dropped below 8 AIU. Total loss of the fluorescent signal was not achieved for any trial. However, the 40xArch trial displayed faint fluorescence at the end of its testing period, just a few points above the background fluorescence. Conversely, the 10xArch test still showed bright fluorescence after the full duration of the experiment and was, overall, the least affected by photobleaching. This was true despite the fact that its fading rate within the first 10 minutes was comparable to the 10x and 20x modern trials. Regardless of the age of the fluorescent label, the loss of fluorescence intensity over time for each objective obeyed a simple first order single-exponential model (Table 1). The trend's fit was

evidenced by R2-values above 0.94, for all trials except 40xArch (R2=0.89). Closer examination of residuals between the observed data and the fitted curve reveal that archaeological samples deviate somewhat from the expected single-exponential trend.

Table 1.1: Photobleaching rates and R^2 values for modern TC controls and archaeological fluorescence. Data for all trials fit exponential trends over the total scanning time. Residual plots however, demonstrate that photobleaching trends in archaeological trials deviates from a single-exponential function.

		Exponential [y=ac-b(t)]	
Sample Set	Objective	Rate	R^2
Modern	10x	$3.9e^{-4}$ min^{-1}	0.95
	20x	$4.1e^{-4}$ min^{-1}	0.99
	40x	$5.7e^{-4}$ min^{-1}	0.96
Archaeological	10x	$2.5e^{-4}$ min^{-1}	0.94
	20x	$2.9e^{-4}$ min^{-1}	0.95
	40x	$3.8e^{-4}$ min^{-1}	0.89

For both archaeological and modern tests, higher-powered objectives induced more rapid rates of photobleaching. The 10x objective induced photo bleaching of the modern label at a rate of $3.9e^{-4}$ min^{-1} and the archaeological at $2.5e^{-4}$ min^{-1}. The 20x objective induced photobleaching at a more rapid rate of $4.1e^{-4}$ min^{-1} in the modern and $2.9e^{-4}$ min^{-1} in the archaeological samples. In comparison, the most drastic photobleaching occurred using the 40x oil immersion objective at rates of $5.7e^{-4}$ min^{-1} and $3.8e^{-4}$ min^{-1} for modern and archaeological samples respectively.

Fluorescence from modern samples faded at a faster rate than archaeological samples regardless of the objective used. Modern labels had an average photobleaching rate of $4.6e^{-4}$ min^{-1}, whereas archaeological samples had an average rate of $3.1e^{-4}$ min^{-1}. Though this is true over the total time measured, within about the first 10 min of scanning

the archaeological samples actually fade in intensity more rapidly, especially at higher objectives.

Discussion and Conclusion

These results verify our hypotheses and demonstrate that confocal laser scanning microscopic spectral analysis is a beneficial tool for fluorescence spectrum and intensity measurement in bone tissue. CLSM spectral analysis allowed the identification and isolation of emitted light from fluorochromes present in dyed decalcified dog bone; tetracycline labeled modern pig bone; and archaeological, human bone from the Kellis sites of the Dakhleh Oasis, Egypt. Spectra from modern samples and archaeological samples had the same peak fluorescent intensities, corresponding to expected values from the literature. Background fluorescence was negligible during the comparison of fluorescent spectra and intensities and the archaeological slide preparation process was shown to be more suitable for fluorescence analysis. Photobleaching tests demonstrated that for normal imaging (less than two minutes of required scanning time), fluorescence decay is minimal.

In response to 458 nm laser excitation, fluorescence observed in the decalcified dog bone (negative for TC) should be representative of collagen or eosin, a chemical stain used in the sample preparation. Collagen Type I has a peak at 364 nm in response to 218 nm excitation (Yu-Hua et al. 1997). Stained decalcified dog bone displayed a spectrum sharply peaked at 562 nm (at 458 nm excitation), similar to that of eosin, reported to peak at 550-560 nm in response to 450 nm excitation (Raymo et al. 2004).

Therefore CLSM spectral analysis accurately described this fluorochrome's spectrum. The contribution of collagen was not visible as a separate peak for any sample due to its inefficient excitation at 458 nm in comparison to other fluorochromes present.

Modern, TC labeled pig bone and human archaeological bone fluorescence both displayed bright green-yellow fluorescence with emission peaks at 525 nm. Other studies on the typical spectral characteristics of modern TC report peak emission wavelengths at 520-530 nm (Fukutani et al. 1985) and for archaeological fluorescence at 525 nm (Cook et al. 1989). Results of the current study provide quantitative corroboration for previous identifications of archaeological TC labels made by label morphology, standard UV-B epifluorescence microscopy, and spectroscopy, supporting the observation that tetracyclines were somehow incorporated into the skeletons of ancient Roman-Egyptians, in life or after death.

The contribution of the baseline and background fluorescence to that of fluorescent labels was negligible in both modern and archaeological bone. Archaeological samples provided a more homogenous baseline and background emission. This was not expected because it was assumed that archaeological bone would be "dirtier" and that scattering of light from sedimentary and crystalline deposits within the bone could increase collection of meaningless light. Also unexpected, intensity analysis shows most non-label light collected was not due to background fluorescence of bone but to the baseline. Visually, baseline ROIs were solid black in the microscope. This hints that for some reason the non-detection point is not at zero, but ~3 AIU for samples investigated here (likely due to an artifact generated by the detector specifications).

Though slight in general, contamination from background and baseline fluorescence was more significant in the modern samples at <527 nm, increasing in intensity it neared the laser line at 458 nm. Because samples were nearly equal in thickness, and because CLSM only collects light from one focal plane, this effect is probably related to photochemical or optical properties of the embedding material used for these samples. Therefore, during CLSM imaging and spectral analysis of bone, the Biodur® preparation technique could be preferable, contributing both more predictable and lower levels of non-label fluorescent "noise".

The current research showed photobleaching of TC labels in bone is possible during CLSM, especially while using increased laser power, stronger objectives, and scanning zoom. The rate of photobleaching increased when more powerful objectives were used because they focus more light on a smaller area of sample, thereby inducing more excitation/emission cycles in fewer molecules. Despite this observation, continuous scanning would have to take place at the same field of view for longer than 10 minutes in order to lose 50% of the intensity of a label, even at 400x magnification. Power settings and scanning zoom were employed specifically to increase the rate of photobleaching; otherwise an hour of scanning time was not enough to observe trends. Even under these circumstances, photobleaching is only a minor limitation for bone fluorescence analysis at objectives ≤40x because most imaging or spectral analysis can be accomplished in under two minutes of scanning.

Despite similarities, measurable differences between modern and archaeological TC fluorescence exist. Spectral curves for archaeological labels are less intense, less sharply peaked, and have a wider range of emission. This could be due to the presence of

multiple forms of TC, several of which are naturally produced by different species of bacteria (for example chlortetracycline from *Streptomyces aureofaciens* versus oxytetracycline from *S. rimosus*) (Goodfellow et al. 1988). Each form of TC has characteristic differences in emission peak or spectral curvature (Hoerman 1975), when combined, their effects could both account for the wider range of emission and the altered photobleaching rate seen in archaeological trials. The current study suggests photobleaching trends for all samples fit the expected function for single-exponential decline (as each molecule fatigues the rate of photobleaching decreases because there are fewer left to bleach). That being said, archaeological samples bleach at a function that is less exponential – nearly logarithmic. This finding is especially clear during the first ten minutes of scanning where a first order function seems most inaccurate, as evidenced by the residuals plots for the photobleaching tests. Song and fellow researchers found that one or several bimolecular photochemical reactions can cause significant deviations from single-exponential functions describing unimolecular processes (Song et al. 1997). However, bimolecular reactions in this complex solid media with low fluorochrome density may be unlikely.

Another possibility is that over 1,700 years of environmental change, TC molecules have undergone chemical modification. Originally cited in Keith and Armelagos (1988), Boothe suggested this likelihood in 1983 regarding the evidence from Sudan, but the manuscript was never published. Though the byproducts of environmentally degraded, bone-bound TC are unknown, some could be fluorescent (though most alterations to fluorochromes reduce their photoreactivity), the environment would provide ample association with Ca^{2+} from bone, a known enhancer of steady-state

fluorescence intensity (Hoerman 1975; Schneider S et al. 2001). Variations in observed photobleaching rates could also be due to slight changes in the refractive index of different embedding solutions (Van Oostveldt et al. 1998), but whether this alters the actual function of bleaching is unclear. Further study using standardized sample preparation and bone type in a photo-kinetics assay would be necessary to definitively account for influences affecting variation in spectral characteristics and photobleaching decay during excitation.

Future investigations could also utilize more versatile laser systems capable of inducing true UV excitation at the wavelength best suited for TC excitation (~390 nm) (Hoerman 1975), possibly for collagen excitation as well. However, the current study corroborates previous research demonstrating that 458 nm laser excitation is fitting for TC fluorescence analysis and imaging. In addition, the combined use of CLSM spectral identification and chemical TC extraction could allow distinction between different forms of bone-bound TC or aid in concentration determination.

Despite evidence that TC labeling in ancient bone is premortem (Basset et al. 1980; Keith and Armelagos 1983; Cook et al. 1989; Armelagos 2000; Maggiano et al. 2003), other reports note that postmortem effects can account for bone fluorescence (Piepenbrink 1983). More information should also be collected on "non-tunneling" bacterial and fungal bone invasion. Not all microorganisms leave behind visible damage in the form of tunnels through the bone (Hackett 1982), tertiary decomposers like those producing TC included (Goodfellow et al. 1983). In the future, CLSM could be useful for the quantification of trends in bone discoloration and fluorescence, targeted microbial

damage, and sedimentary deposits – enabling discrimination between postmortem and premortem TC exposure from archaeological skeletal remains.

Confocal laser scanning microscopy has many advantages over standard forms of bone microscopy for fluorescence and morphological analysis of bone. These include improved z-axis resolution, three-dimensional imaging, and spectral analysis. Measurement of bone fluorescence characteristics using CLSM removes artifacts from sample thickness and allows targeted identification of fluorochromes based on spectral characteristics. Unfortunately its application to the investigation of hard tissues in general has been rare, especially in archaeology. The results of this project encourage the development, standardization, and implementation of CLSM techniques for fluorescence spectral analysis and imaging in medical and anthropological sciences and suggest CLSM as an appropriate tool for the investigation of ancient tetracycline fluorescence in human bone.

References

Armelagos GJ. 2000. Take two beers and call me in 1,600 years. Natural History 109(4):50-4.

Bassett E, Keith M, Armelagos GJ, Martin D, and Villanueva A. 1980. Tetracycline-labeled human bone from ancient Sudanese Nubia (A.D. 350). Science 209:1532 -34.

Biggerstaff J, Amirkhosravi A, and Francis JL. 1997. Three-dimensional visualization and quantification of fibrin in solid tumors by confocal laser scanning microscopy. Cytometry 29(2):122-7.

Biggerstaff J, Amirkhosravi A, and Francis JL. 1998. Three-dimensional quantitation of tumor microvessel density by confocal laser scanning microscopy. Cell Vision. Journal of Analytical Morphology 4(2):152-3.

Birkenhäger-Frenkel DH and Birkenhäger. 1987. Bone appositional rate and percentage of doubly and singly labeled surfaces: comparison of data from 5 and 20 µm sections. Bone 8(7):7-12.

Boyde A, Babayemi J, Jones SJ, and Wolfe LA. 1994. P37 Improved spatial and temporal resolution in tetracycline and calcein labeling in bone and dentine. Bone 15(4):460.

Burr DB, Martin RB, and Sharkey NA. 1998. Anlaysis of bone remodeling in skeletal tissue mechanics. New York: Springer-Verlag.

Cahalan MD, Parker I, Wei SH, and Miller MJ. 2002Two-photon tissue imaging: seeing the immune system in a fresh light. Nature Reviews: Immunology 2:874.

Carr AB, Gerard DA, and Larsen PE. 1996. The response of bone in primates around unloaded dental implants supporting prostheses with different levels of fit. Journal of Prosthetic Dentistry 76(5):500-9.

Carr AB, Gerard DA, and Larsen PE. 1996. Histomorphometric analysis of implant anchorage for 3 types of dental implants following 6 months of healing in baboon jaws. International Journal of Oral Maxillofacial Implants 15(6):785-79.

Cook M, Molto E, and Anderson C. 1989. Fluorochrome labelling in Roman period skeletons from Dakhleh Oasis, Egypt. American Journal of Physical Anthropology 80(2):137-43.

Eriksen EF, Axelrod DW, and Melsen F. 1994. Bone histomorphometry. New York: Raven Press. 1-67.

Frost HM. 1965. Tetracyclines and fetal bones. Henry Ford Hospital Medical Journal 13(4):403-10.

Frost HM, Villanueva AR, Roth H, and Stanisavljevic S. 1961. Tetracycline bone labeling. The Journal of Clinical Pharmacology 1:206-16.

Fukutani S, Tsukamoto Y, and Mori M. 1985. Determination of fluorescent oxytetracycline complexes in dental and skeletal hard tissues by rapid and accurate quantitative method. Progress in Clinical and Biological Research 187:215-24.

Gilbertson-Beadling S, Powers EA, Stamp-Cole M, Scot PS, Wallace TL, Copeland J, Petzold G, Mitchell M, Ledbetter S, Poorman R, Wilks JW, and Fisher C. 1995. The tetracycline analogs minocycline and doxycycline inhibit angiogenisis in vitro by a non-metalloproteinase-dependent mechanism. Cancer Chemotherapy and Pharmacology 36:418-24.

Goodfellow M, Mordarski M, and Williams ST. 1983. Biology of the Actinomycetes. New York: Academic Press Inc.

Goodfellow M, Williams ST, and Mordarski M. 1988. Actinomycetes in Biotechnology. New York: Academic Press Inc.

Hackett CJ. 1981. Microscopical Focal Destruction (Tunnels) In Exhumed Human Bones. Medicine, Science and the Law 21:243-265.

Hoerman KC. 1975. Spectral characteristics of tetracycline-induced luminescence in rat teeth and bones. Journal of Dental Research 54:131-6.

Hope C A. 2001. Observations on the dating of the occupation at Ismant el-Kharab, In C. A. Marlow and A. J. Mills, editors. The Oasis Papers 1: The Proceedings of the First Conference of the Dakhleh Oasis Project. Oxford: Oxbow Books pp.43–59.

Horvath JJ and Glazier SA. 1993. Fluorescence measurements of tetracycline in high cell mass for fermentation monitoring. American Biotechnology Laboratory 11(7):44.

Johnson RH and Mitchell DF. 1966. The effects of tetracyclines on teeth and bones. Journal of Dental Research 45(1):86-93.

Keith M and Armelagos GJ. 1983. Naturally occurring antibiotics and human health. In: Romanuuci L, Moerman D, and Tancredi L, editors. The Anthropology of Medicine. New York: Bergin and Garvey Publishers pp.68-79.

Keith M and Armelagos GJ. 1988. An example of in vivo tetracycline labeling: Reply to Piepenbrink. Journal of Archaeological Science 15:595-601.

Maggiano C, Dupras T, and Biggerstaff J. 2003. Ancient antibiotics: evidence for tetracycline in human and animal bone from kellis. In: Mills AJ and Hope CA, editors. The Dakhleh Oasis Monograph. vol.3. Oxford: Oxbow Books pp.331-344.

Milch RA, Rall DP, and Tobie JE. 1957. Bone localization of tetracyclines. Journal of the National Cancer Institute 19(1):87-93.

Milch RA, Rall DP, and Tobie JE. 1958. Fluorescence of tetracycline antibiotics in bone. The Journal of Bone and Joint Surgery 40(4):897-910.

Misra DN. 1991. Adsorption and orientation of tetracycline on hydroxyapatite. Calcified Tissue International 48(5):362-7.

Molto J E. 2001. The comparative skeletal biology and palaeoepidemiology of the people from Ein Tirghi and Kellis, Dakhleh Oasis, Egypt, in C. A. Marlow and A. J. Mills, eds, The Oasis Papers 1: The Proceedings of the First Conference of the Dakhleh Oasis Project. Oxford: Oxbow Books pp.81–100.

Nielsen P and Gyrd-Hansen N. 1996. Bioavailability of oxytetracycline, tetracycline, and chlortetracycline after oral administration to fed and fasted pigs. Journal of Veterinary Pharmacology and Therapeutics 19(4):305-11.

Ono M, Murakami T, Kudo A, Isshiki M, Sawada H, and Segawa A. 2001. Quantitative comparison of anti-fading mounting media for confocal laser scanning microscopy. The Journal of Histochemistry and Cytochemestry 49(3):305-11.

Piepenbrink H, Herrmann B, and Hoffman P. 1983. Tetracylintypische fluoreszenzen and bodengelagerten skeletteilen. Zeitschrift fur Rechtsmedizin 91:71-4.

Raymo FM and Tomasulo M. 2004. Electron and energy transfer modulation with photochromic switches. Chemical Society Reviews 34:327-36.

Rush T, Pirok D, and Frost HM. 1966. Fractional labeling: the fraction of actively forming osteons that take tetracycline labels in normal human bone. Henry Ford Hospital Medical Bulletin 14:255-263.

Sadowski T. and Steinmeyer J. 2001. Effects of tetracyclines on the production of matrix metalloproteinases and plasminogen activators as well as of their natural inhibitors, tissue inhibitor of metalloproteinases-1 and plasminogen activator inhibitor-1. Inflammation Research 50(3):175-182.

Saxen L. 1966. Drug-induced teratogenesis in vitro: inhibition of calcification by different tetracyclines. Science 153:384-7

Schneider S, Schmitt M, Brehm, Reiher M, Matousek P, and Towrie M. 2003. Fluorescence kinetics of aqueous solutions of tetracycline and its complexes with Mg^{2+} or Ca^{2+}. Photochemical and Photobiological Sciences 2(11):1107-17.

Stout SD. 1978. Histological structure and its preservation in ancient bone. Current Anthropology 19(3):601-604.

Schultz M. 1988. Methoden der Licht- und Elektronenmikroskopie. In: Knußmann R, editor. Anthropologie: Handbuch der vergleichenden Biologie des Menschen. Stuttgart: Fischer Verlag 1(1):698–730.

Schultz M. 2001. Paleohistopathology of bone: a new approach to the study of ancient diseases. Yearbook of Physical Anthropology 44:106–147.

Skinner HC and Nalbandian J. 1975. Tetracyclines and mineralized tissues: review and perspectives. Yale Journal of Biology and Medicine 48(5):377-97.

Song L, van Gijlswijk RPM, Young IT, and Tanke HJ. 1997. Influence of fluorochrome labeling density on the photobleaching kinetics of fluorescein in microscopy. Cytometry 27:213-23.

Stout SD and Teitelbaum. 1976. Histological analysis of undecalcified thin sections of archaeological bone. American Journal of Physical Anthropology 44:263-70.

Taylor T and Frost HM. 1966. The existence of a zone of finite thickness during tetracycline labeling of bone. Henry Ford Hospital Medical Bulletin 14:255-263.

Urist MR and Ibsen KH. 1963. Chemical reactivity of mineralized tissue with oxytetracycline. Archives of Pathology 76(5):484-496.

Van Der Bijl P and Pitigoi-Aron G. 1995. Tetracyclines and calcified tissues. Annals of Dentistry 54(1-2):69-72.

Van Oostveldt P, Verhaegen F, and Messens K. 1998. Heterogeneous photobleaching in confocal microscopy caused by differences in refractive index and excitation mode. Cytometry 32:137-46.

Villanueva AR, Kujawa M, Mathews CHE, and Parfitt AM. 1983. Identification of the mineralization front: comparison of a modified toluidine blue stain with tetracycline fluorescence. Metabolic Bone Diseases and Related Research 5:41-45.

Walsh P. 2000. Physicians' Desk Reference. Montvale, NJ: Medical Economics Company, Inc.

White T D. 2000. Human Osteology, Second ed. New York: Academic Press.

Yu-Hua L, and Jia-Chang Y, and Guo-Ping C. 1997. Fluorescence characterization of type I collagen from normal and silicotic rats and its quenching dynamics induced by hypocrellin B. Biopolymer 42:219-26.

CHAPTER 3

CONFOCAL LASER SCANNING MICROSCOPY: A FLEXIBLE TOOL FOR POLARIZED LIGHT AND THREE-DIMENSIONAL FLUORESCENCE IMAGING OF ARCHAEOLOGICAL COMPACT BONE HISTOLOGY

Introduction

Understanding bone microarchitecture and histology is vital for the prevention, diagnosis, and treatment of modern disease, and for archaeological and forensic investigation including pathological examination, age estimation, and species identification. The basic structural and functional unit of mature compact, or cortical, bone is the osteon. Roughly 200-400 μm in diameter (Soames 1999), osteons can be visualized as layered cylindrical tubes surrounding bone vascular tissue (Figure 3.1).

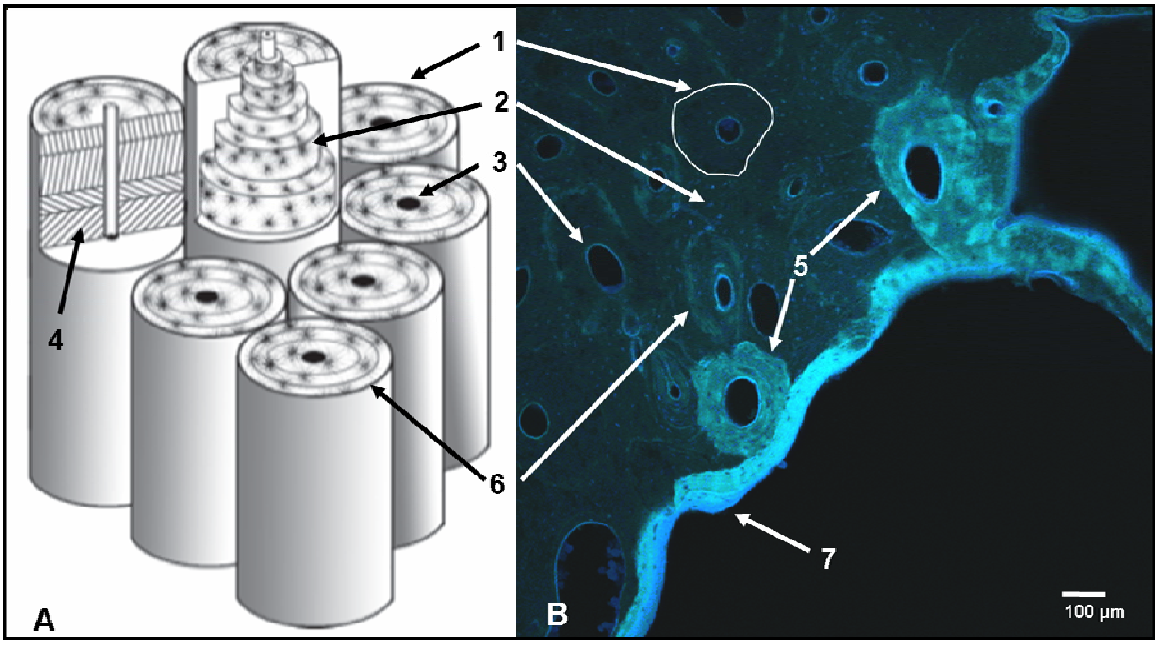

Figure 3.1: Basic microstructure of mature compact bone. A) Cylindrical representations of osteons (courtesy of L. Williams). B) Two-dimensional confocal laser scanning microscopic image of archaeological bone fluorescence from individual D7-8, from the Kellis town site, Dakhleh Oasis, Egypt, showing: 1) non-fluorescent osteon, or Haversian system (white perimeter hand-drawn for clarification), 2) lacunae, 3) Haversian canal wall, 4) alternating orientation of organic and mineral lamellae (as described by Ascenzi and Bonnuci in 1968), 5) two completely fluorescent osteons, 6) cement line or reversal line, and 7) fluorescently labeled internal circumferential lamellae. Scale notes 100um, 100x total magnification.

Osteons have well marked, highly mineralized boundaries in cross section, called cement lines, separating them from surrounding older bone tissue. On a larger scale, they are organized into multiple generations of longitudinally organized networks dominated by branching events and horizontal connections called Volkmann's canals (Stout et al. 1999; Cooper et al. 2003). Each osteon is formed by concentric apposition of layers of calcified matrix called lamellae. Lamellae form from the outside periphery of the osteon, the cement line or reversal line, toward the vascular canal at the center. In life, osteon formation occurs in a multicellular unit referred to as a bone remodeling unit, or BRU (Eriksen et al 1994) (sometimes referred to as a basic multinuclear unit (Mohsin et al.

2002) which moves through less mature bone resorbing bone at the leading end, or cutting cone (Burr et al. 1998), and appositionally depositing new tissue around vascular structures at its closing cone (Jaworski 1992). Some osteocytes lock themselves within cavities called lacunae positioned between lamellae. Lacunae are connected via radially oriented crack-like tunnels, or canaliculi, thus supplying bone distant from vessels with nutrient. In a normal individual, osteons result from a total modeling period lasting roughly 100 days (Eriksen et al. 1994) and have estimated lengths of 0.001 to 2.5 mm (Cohen and Harris 1958; Eriksen et al. 1994).

An understanding of this anatomical system has been pieced together over many years of bone microscopy, or histomorphometry, during which morphologically distinct osteon types have been noted (Richman et al. 1979; Robling and Stout 1999; Stout et al. 1999). Some are now known to be artifacts of two-dimensional (2-D) thin sectioning and others are poorly understood, even from a structural perspective. Compact bone is an optically dense, dynamically evolving, organic and mineral tissue comprised of multiple generations of layered tubular networks interconnected by branching and bridging; the fact that 2-D imaging of bone can be problematic should not be surprising.

Taking advantage of the unique composition and formation characteristics of hard tissues, many techniques have been developed to gain insight into the microarchitecture of hard tissues. Specifically, polarized light microscopy, epifluorescence microscopy, and seriated thin-ground sectioning have illuminated many aspects of bone formation, modeling, and remodeling as well as the processes of disease and biomechanical adaptation (Schultz 2001).

Polarized light microscopy creates an image based on the sample's ability to refract light at multiple indices. This property is called birefringence and in bone differentially illuminates lamellar structure, dependant on the orientation of collagen (positively birefringent) and mineral (negatively birefringent) (Boyde and Riggs 1990; Bromage et al. 2003). The most common forms of this technique employ linearly polarized light resulting in an interference pattern in osteons that has been referred to as the "Maltese cross". This cross remains in place as the sample or polarizers are rotated, allowing illumination of all of the tissue but never all of the tissue at a single stationary position (Boyde et al. 1984).

Wide-field epifluorescence microscopy is another invaluable tool used in bone histomophometry, marking living bone with fluorescent labels such as tetracycline (TC) (Milch et al. 1957, 1958). Multiple labels can be created in bone, marking the time period between old and new bone growth, and measuring changes in bone structure over time (Frost et al. 1961; Frost 1965; Rush et al. 1966; Taylor and Frost 1966; Villanueva et al. 1983). Tetracycline fluorescence has also been discovered in untreated human bone recovered from several archaeological sites in Egypt (ranging from around 100 B.C.E to A.D 400) (Cook et al. 1989; Maggiano et al. 2003) and in Sudan (A.D. 350) (Basset et al. 1980; Keith and Armelagos 1983, 1988; Armelagos 2000). However, many questions regarding these "ancient antibiotic" labels have been raised regarding the mechanism for premortem exposure (Armelagos 2000), possible health effects (Maggiano et al. 2003), and the degree of postmortem fluorescence contribution due to microbial diagenesis (Piepenbrink et al. 1983).

The major limitation of polarized light and standard epifluorescence microscopy is that the offered perspective is two-dimensional (2-D) in a quite literal sense. Laborious, serial thin sectioning, even when aided by computerized imaging techniques, destroys three-dimensional (3-D) information at a function of the distance between each slice. High-resolution micro-computerized tomography (μCT) is bringing a more holistic perspective to analysis of bone porosity and strength (Wachter et al. 2001; Wachter et al. 2002; Cooper et al. 2003). Unfortunately μCT will never be able to label generations of bone growth as with fluorescence techniques, nor is it capable of imaging general collagen preservation or bone strength properties via polarized light. In addition, μCT is limited by its inability to differentiate between solid structures and their interfaces (Cooper et al. 2003), whereas microscopic techniques allow internal structures such as cement lines, lamellae, lacunae, and canaliculi to be viewed easily.

Encountering some of the same difficulties with wide-field microscopy and unable to use μCT, cell biologists and soft tissue histologists are turning to confocal laser scanning microscopy (CLSM) to reform standing assumptions regarding tissue and cellular structure (Jouk et al. 1995; Rodriguez et al 2003) and biochemical interaction (Biggerstaff 1997, 1998). Between older forms of microscopy and newer tomographic techniques, rests a largely neglected application for confocal laser scanning microscopy (CLSM): histomorphometry of compact bone.

Despite potential benefits, CLSM is still rarely employed for bone tissue imaging and its application in archaeological and forensic sciences is especially neglected. The intent of the current study is to call attention to some of the well-known but not well-communicated benefits CLSM techniques could have for bone histomophometry. Well

preserved archaeological bone from the Dakhleh Oasis, Egypt was examined using a confocal laser scanning microscope. Results are compared with those of standard wide-field epifluorescence and polarized light systems. Modern alveolar pig bone labeled with tetracycline was used for fluorescence controls. Of particular interest was determining what types of imaging techniques are simultaneously possible in separate "channels" of collected light, and what 3-D CLSM imaging may contribute to the study of compact bone microarchitecture.

Materials and Methods

Sample collection and processing

Archaeological skeletal remains were selected from the Kellis 2 cemetery and Kellis town site of the Dakhleh Oasis, Egypt, *circa* AD 100-400 (Hope 2001; Molto 2001). Studies from sites in Sudan and Egypt report that nearly every individual skeleton displays some evidence of fluorescence (Bassett et al. 1980; Keith and Armelagos 1983, 1988; Cook et al. 1989; Maggiano et al. 2003). Six individuals were examined, B443, B431, B116, D7-8, B393, and B427. Transverse cross sections were removed from these adult skeletons at the mid-diaphysis of the left humerus during DNA and stable-isotope sampling. Slides were prepared from this location to ensure presence of ample compact bone and to limit the number of skeletal elements affected by sampling.

Observation from previous studies suggested lacunar and Haversian wall fluorescence is prevalent in nearly every archaeological sample investigated, whether the osteon is otherwise labeled or not. It was thought this could be some form of edge-effect

illumination due to imaging artifacts created by the embedding procedure (Maggiano et al. 2003). Therefore, for this study, thin-ground sectioning was performed using Hagens' Biodur® plastination technique as altered by Schultz and Brandt (Schultz 1988, 2001). This technique, though requiring more preparation time, provides optimum penetration of micro-porous structures and seamless joining with internal and external microscopic surfaces, eliminating many possible artifacts and prolonging the "lifetime" of the sample indefinitely (Schultz 1988, 2001). Previous studies show background and TC label fluorescence alone is sufficient for CLSM imaging with no additional treatment necessary (Maggiano et al. 2003). Slides produced were 70 μm or ~140 μm thick (as measured by micrometer before cover-slipping).

All samples were analyzed for diagenesis and pathology at the Zentrum Anatomie, Geörg-August-Universität, Göttingen, Germany. Original internal and external surfaces were intact, postmortem fragmentation and micro-fracture were absent, and no signs of generalized chemical or biological destruction were found. Localized artifacts of diagenesis in ancient bone are unavoidable, but overall sample preservation was excellent. Other studies on ancient bone from similar dry, sandy environs suggested organic and mineral preservation in bone could be similar in quality to that of modern biopsy tissue (Keith and Armelagos 1988). Slides selected for this study were also negative for obvious infectious metabolic or degenerative disease. Drawings were made from a magnifying projector and key features were microphotographed.

In addition, sections from modern pig alveolar bone from were used as positive controls for fluorescence in bone due to tetracycline labeling (generously provided by Dr. David Gerard, University of Tennessee, Knoxville). These samples were prepared using

standardized methods for TC double labeling techniques (Carr et al. 1996a, 1996b). Dr. Richard Smith at the University of Tennessee, Memphis, contributed similar control sections from rabbit distal femora that were used for the optimization of current procedures.

Confocal microscopic imaging of compact bone

A Leica SP2 confocal laser scanning microscope was used for all CLSM imaging. In comparison with wide-field microscopy, modern CLSM provides greater z-axis resolution and 3-D reconstruction of tissues over 100 μm in thickness (Biggerstaff et al. 1997, 1998; Boyde et al. 1994, Maggiano et al. 2003). These feats are achievable due to several unique principles of confocal microscopy. First, confocal systems use extremely bright and finely focused lasers (~0.2μm in diameter) to provide incident illumination. A computerized operating system manipulates mirrors, rapidly scanning the laser across the focal plane and inducing excitation in the target fluorochrome(s). Second, diffuse out-of-focus light from above and below the focal plane, is refocused either before or after an adjustable pinhole, permitting collection of only light from the target focal plane. This plane can be moved up or down within the sample, creating 3-D stacks or to simply view any depth without the influence of out-of-focus light. An electronically controlled crystalline filter, called an acousto-optical tunable filter (AOTF), organizes collected light, permitting only desired wavelengths to reach the photon detector(s). This component is increasingly common in CLSM systems and allows precise selection of desired wavelengths used for excitation of fluorochromes and detection of emitted light, whereas standard epifluorescent systems use non-tunable beam splitters and filters that

must be changed manually. Finally, the computer correlates photon impacts with the laser's scanning position and uses this information to create a digital image of the fluorescence in the sample, in this case fluorescence emitted by tetracycline.

Fluorescence response of TC was achieved using an argon ion laser light source set for 458 nm excitation. The excitation peak for TC is around 390 nm (Hoerman 1975). Studies using CLSM, however, have shown that laser excitation at 458 nm induces ample excitation of modern TC labels *and* ancient fluorescence in bone (Boyde et al. 1994; Takeshita et al. 1997; Maggiano et al. 2003). Detection of multiple fluorescence and scattered light channels was accomplished using an acusto-optical tunable filter (AOTF). Relatively high laser power was used (100% software setting, 25% manual) in order to decrease the amount of photon multiplication necessary for image generation. Contrast stretching using the Leica® "LUT" settings ensured systems configuration was not used to distort the dominance of features due to over or under exposure (detector saturation or non-detection).

For efficiency, the CLSM system's wide-field epifluorescence mode was used to locate fields of interest. Preferred fields of interest contained, ring fluorescence or thicker labels such as complete osteon fluorescence or fluorescence of the internal/external circumferential or tangential lamellae. Also of interest were: double zonal osteons, drifted osteons, Volkmann's canals, non-Haversian canals, branching events and other structures particularly interesting for confocal imaging in three dimensions.

Digital reconstruction of a volume of bone using CLSM is accomplished by stepping the focal plane and objective down through the sample, taking progressive scans

at sub-micron serial intervals. These scans are combined to create a 3-d image, or "z-stack". Roughly half to one third of the Leica® Confocalsoftware's suggested number of scans was used during the creation of each three-dimensional bock, due to file size limitations (especially during high magnification, high resolution imaging). Imaging parameters such as objective, beam splitter, laser power, pinhole size, photomultiplier sensitivity, z-position, pixel/voxel dimensions, emission detection range, and the number of scans were recorded for each image. ImagePro® software was used for measurements and animation.

Results

Two-dimensional imaging

CLSM was capable of generating images using multiple channels of detected light. This could be accomplished for 2-D or 3-D imaging. During CLSM fluoresence imaging, a separate channel of polarized light could also be collected. Results of PLM using laser illumination were similar to images produced using standard bright-field incident light on a non-confocal microscope except that it seemed to produce higher in contrast images (Figure 3.2).

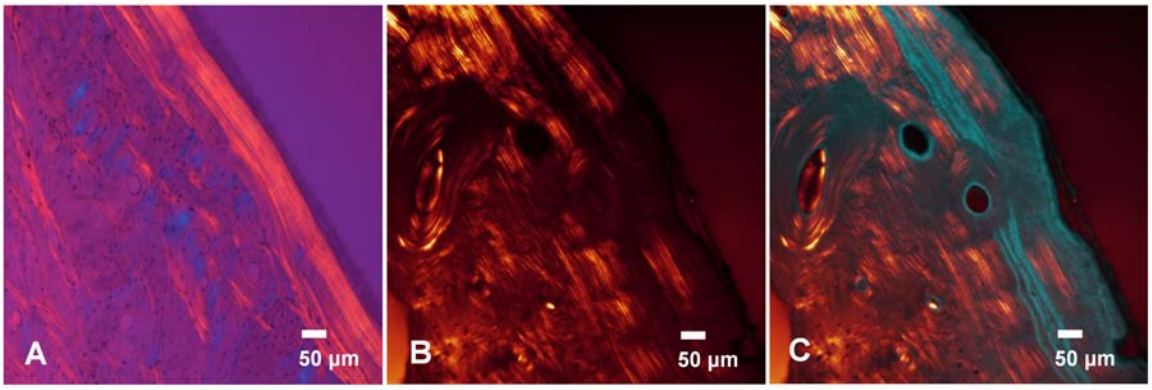

Figure 3.2: Polarized light imaging of undecalcified human compact bone from the left humerus of Burial 431, Kellis 2 Cemetery, Dakhleh Oasis Egypt (circa AD 100-400). Digital images of "lamellar" fluorescence generated using A) red-quarts Hilfsobject enhanced cross-polarized microscopy and B) confocal laser scanning cross-polarized transmission. C) Simultaneous overlay of fluorescence and polarized light channels from the confocal microscope. Cross section is ~70µm thick. Confocal excitation induced by an argon ion laser at 458nm. Scale marks 50 µm.

Bone illuminated in this fashion displayed characteristic alternating laminations of positive and negative birefringence corresponding to predicted positions of organic and mineral bone components. Also clearly visible were dark interference zones where no birefringence was visible depending on the orientation of the sample and polarizing filters. In osteons, the typical "Maltese cross" was evident. Regardless of the structure observed, individual lamellae were distinct and well lit. Clarity of the polarized, laser-scanned image was dependent on the thickness of the sample. Birefringence was visible in samples ~140 µm thick, but samples 70 µm thick displayed better focus and image contrast. As the sample increases in thickness, individual lamella revealed by polarization merge or become blurred using either technique.

It was also possible to simultaneously produce an image in scattered light. Similar images of the same field of view were produced independent of the wavelength of incident light (458 nm, 476 nm 485 nm, 517 nm, 630 nm). This was accomplished by

targeting the detection range five to ten nanometers from the laser's wavelength and adjusting photon multiplication to avoid detector saturation (Figure 3.3).

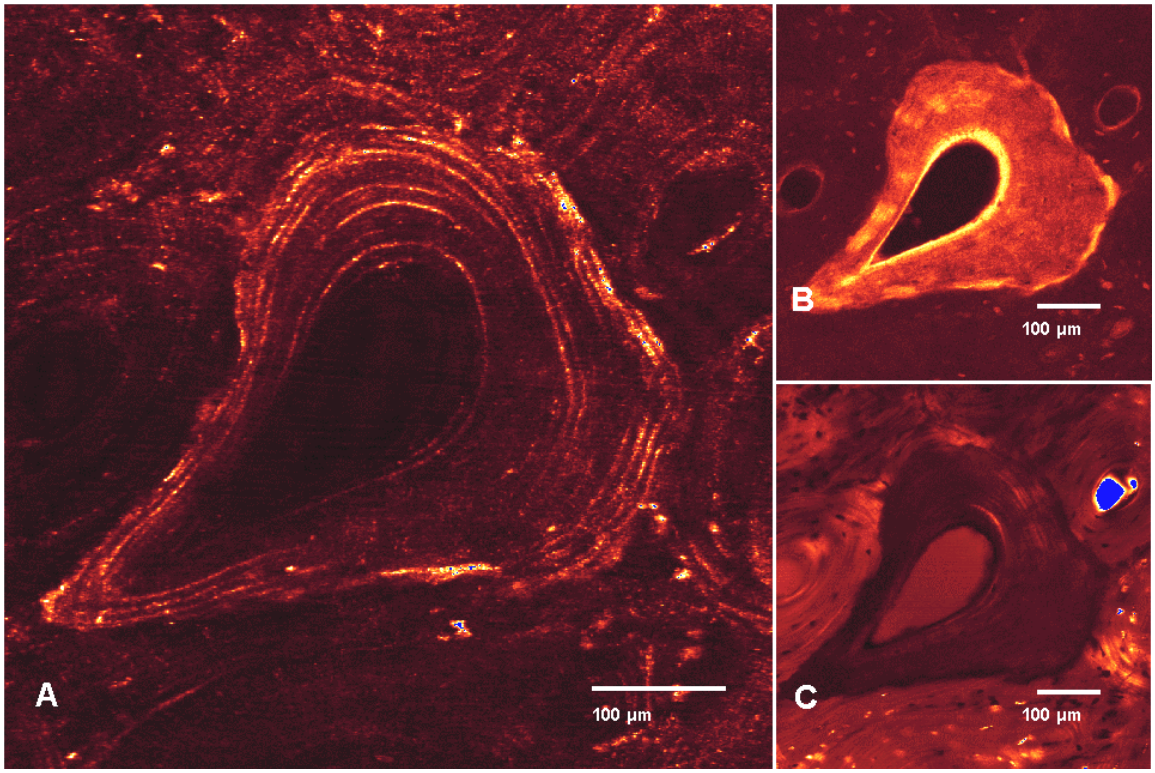

Figure 3.3: Scattered light imaging of a thin-ground section of undecalcified human compact bone from the left humerus of Burial 393, Kellis 2 Cemetery, Dakhleh Oasis Egypt (circa AD 100-400). Digital CLSM images of an oddly shaped osteon (probably due to 2-D artifact at a branching or Volkman's event) in A) scattered light, showing distinct osteonal lamellae and cement lines, B) fluorescent light, and C) linear-polarized transmission. Cross section is ~70 µm thick. Confocal excitation induced by a 458 nm argon ion laser. Scale marks 100µm (2.8x scanning zoom).

The resulting image showed preferential illumination of cement line areas and osteonal lamellae. No interference zones were observed. Small pinpoints of bright light in this channel appeared frequently at the cement line and in lacunae. Like fluorescence channels, scattered light could also be collected in three-dimensions without inclusion of out-of-focus light. Scattered light features seemed to correlate with fluorescent labels.

Fluorescence labels in archaeological samples were more diffuse when imaged using epifluorescence microphotography compared to confocal imaging. Autofluorescence and light diffusion overpowered features such as fluorescent labels, lacunae, and cement lines, especially in thicker samples (~140 µm) (Figure 3.4).

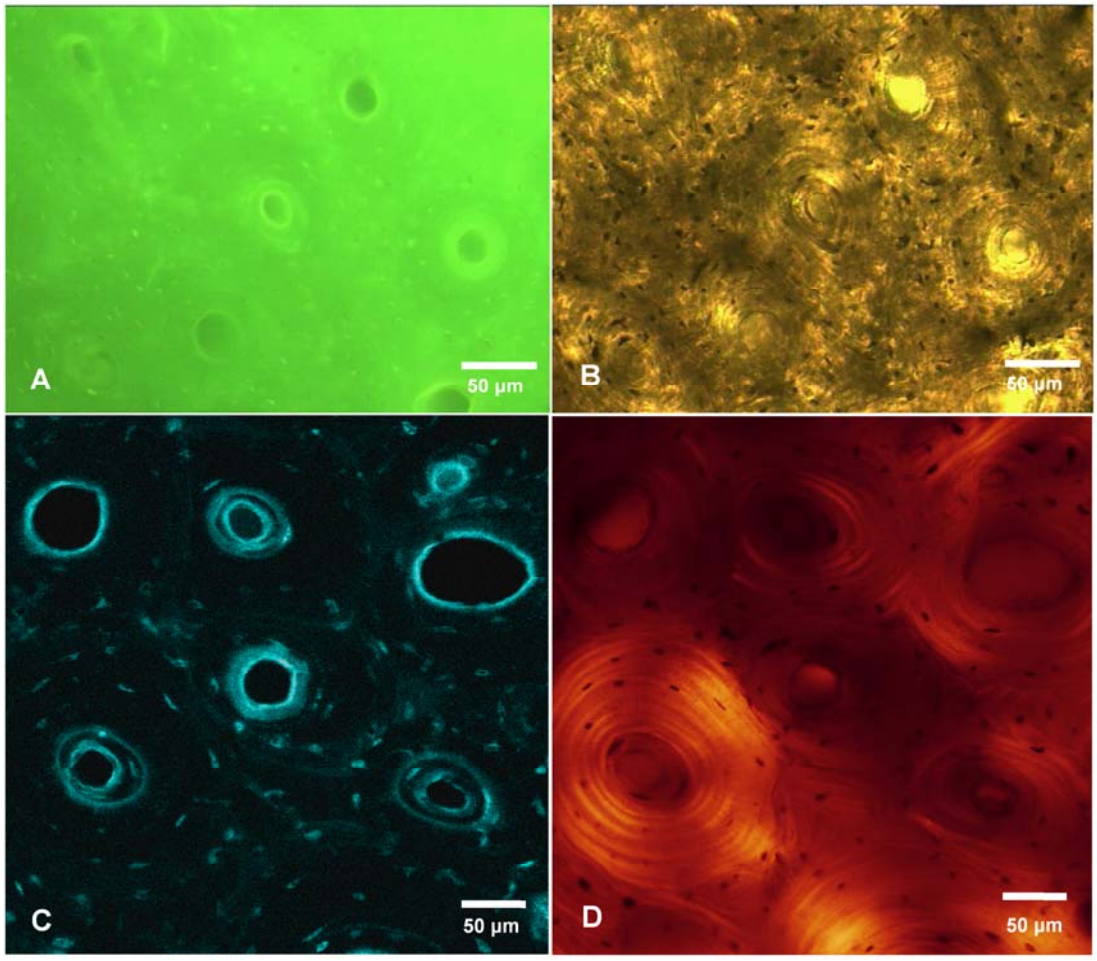

Figure 3.4: Thick-ground section of undecalcified human compact bone from the left humerus of Burial 393, Kellis 2 Cemetery, Dakhleh Oasis Egypt (circa AD 100-400). Digital images of single osteonal "ring" fluorescence generated using UV-B photo-excitation epifluorecence microphotography in A) fluorescent light and B) transmitted light. For comparison, a similar field of view in the same sample was imaged using confocal laser scanning microscopy in C) fluorescent light and D) linear-polarized transmission. Cross section is ~140 µm thick. Confocal excitation induced by a 458 nm argon ion laser. Scale marks 50µm.

In wide-field epifluorescent microphotography, the void within the osteon canal itself was bright despite the fact that there was no bone or soft tissue present there. Independent of exposure time, this equipment could not be optimized optically or digitally to create the clarity produced by CLSM imaging.

In comparison, however, confocal images of compact bone show microscopic fluorescent structures in high contrast and high-resolution. Lacunae, canal walls, and cement lines were oftentimes clearly visible in addition to fluorescent labels. Also, there is an obvious decrease in the number of lacunae within the confocal field of view compared to that of the epifluorescence image. The apparent difference in quality between epifluorescence and CLSM imaging is observed in thin ground sections as well (~70 μm) (Figure 3.5).

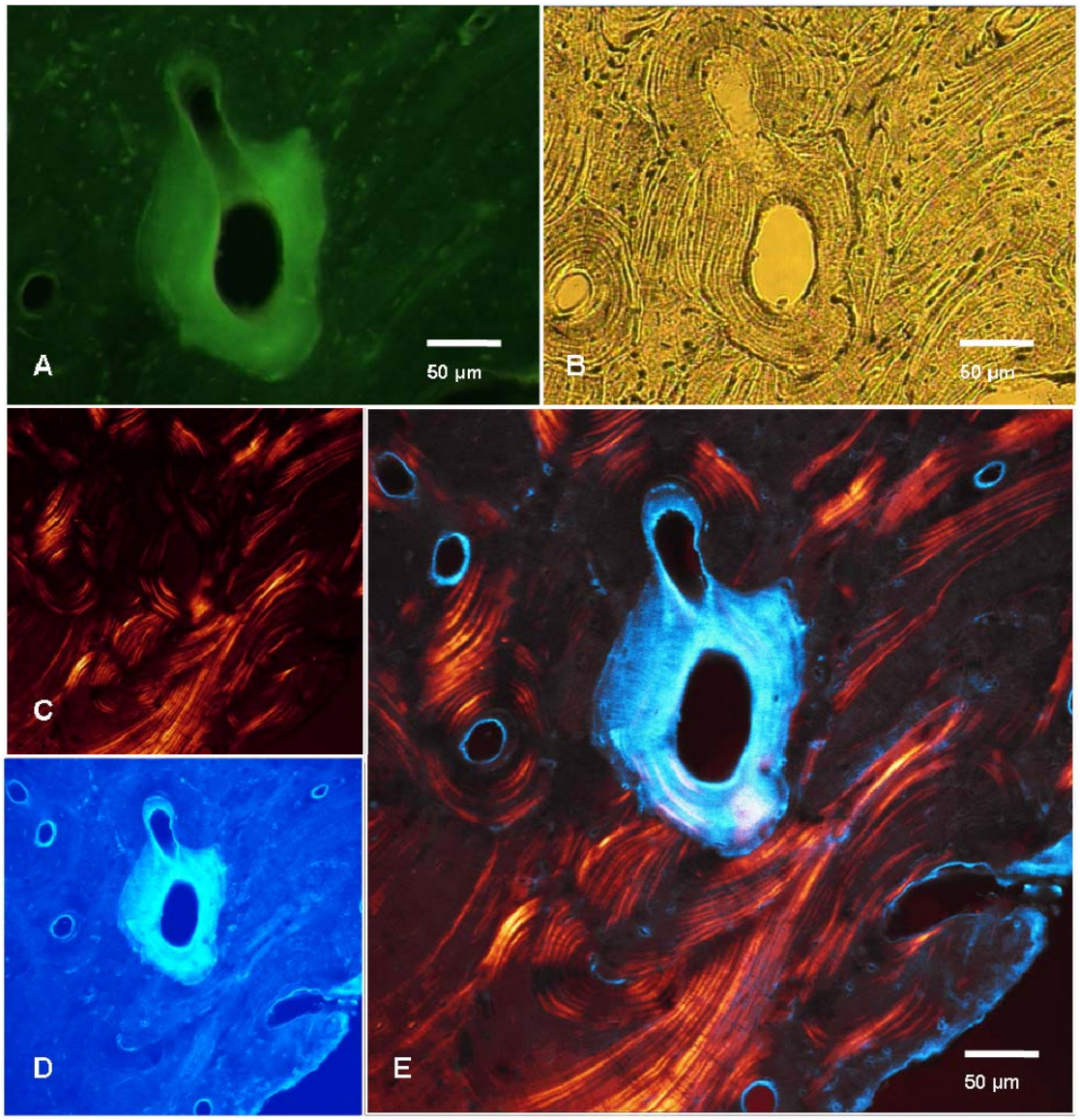

Figure 3.5: Thin-ground section of undecalcified human compact bone from the left humerus of Burial 427, Kellis 2 Cemetery, Dakhleh Oasis Egypt (circa AD 100-400). Digital images of "complete" osteonal fluorescence generated using UV-B epifluorecence microphotography A) in fluorescent light and B) in transmitted light. For comparison, the same osteon was imaged using confocal laser scanning microscopy in C) fluorescent light and D) linear-polarized transmission. E) Simultaneous overlay of fluorescence and polarized light channels. Section is ~70 µm thick. Confocal excitation induced by an argon ion laser at 458 nm. Scale marks 50µm.

This image demonstrates an example of complete fluorescence in one channel (blue) and polarized light in the other (gold). Non-fluorescent structures were not visible

using either CLSM or wide-field epifluorescence microscopy. Overlaying fluorescence and polarized light channels clearly defines the direction of lamellar layers and structural boarders, increasing the visibility of cement lines, lacunae, and even canaliculi.

Three-dimensional imaging

Three-dimensional imaging was achieved to a maximum depth of 115 µm (Figure 3.6).

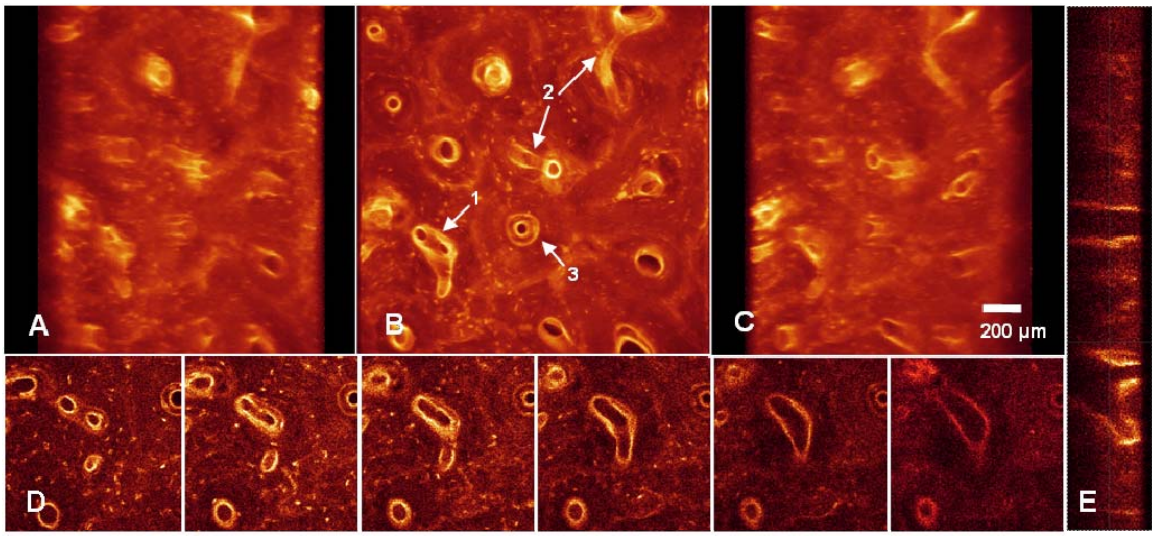

Figure 3.6: Three-Dimensional reconstruction of thick-ground section of undecalcified human compact bone from the left humerus of Burial 393, Kellis 2 Cemetery, Dakhleh Oasis Egypt (circa AD 100-400). Digital 3-D cube generated using confocal laser scanning microscopy and shown from five perspectives A) z-stack left tilt, B) z-stack direct, C) z-stack right tilt, D) Examples of sections from z-stack, E) Orthogonal digital section demonstrating longitudinal view. Also note: 1) non-Haversian canal branching events, 2) Volkman's canals, and 3) "ring" fluorescence and/or double zonal osteon. Digital cross section is ~115 µm thick and imaged using 150 stacked slices at 512x512 pixel2 resolution. Confocal excitation induced by an argon ion laser at 458nm. Scale marks 200 µm.

Signal intensity throughout that thickness was not equal. As the focal plane neared the slide (bottom of the sample) the image faded appreciably, though structural elements such as osteon canals were still visible throughout the fully imaged volume. Cement lines are also clearly visible for much of that depth, as well as lacunae; though both are

best viewed near the top of the z-section. Even canaliculi can be viewed for an appreciable depth of ~30 μm (20x objective, 0.7 NA) and increasing depths (~50 μm) with higher power objectives or better numerical apertures. During z-stack penetration (successive removal of layers from top down) lacunae appear and disappear. Depending on the slice thickness and osteon viewed, sequentially revealed lacunae and canaliculi lend the impression that a single osteon has its own "twist" – not a positional change of the osteon's about its axis of progression, but in its internal components. In several cases "osteon twist" was clockwise in comparison with counter-clockwise neighbors. Under higher power magnification, lightning-like canaliculi can be observed in 3-D radially extending lacuna. Fluorescence in lacunae was normally dominant on one side of the lacunar wall. Not all lacunae were fluorescent however, some appearing as black voids when their walls are not visible (again depending on the magnification).

The most obvious architectural feature revealed by 3-D CLSM imaging is the canal system, the longitudinal Haversian canals and the horizontal Volkmann's canals that connect them. In several z-sections, branching events that connect three or more Haversian canals to a single large canal or resorption area are evident even within ~100 μm of depth. It is also possible to observe trends in osteonal angle across the field of view despite the fact that the cross section is taken perpendicular to the longitudinal axis of the bone. Orthogonal images of z-stacks produce longitudinal sections of 3-D images that are especially suited for determining the angle of osteon continuation relative to the plane of section. Because internal structures of the osteon and its cement lines are evident, distinction can be made between Haversian and non-Haversian canals and resorption areas.

Discussion and Conclusion

Comparison of standard epifluorescence and polarized light enhanced microscopy with confocal laser scanning microscopy (CLSM) demonstrates the advantages of CLSM in imaging undecalcified compact bone sections. During two-dimensional scanning it was possible to detect multiple channels of light simultaneously, separating or overlapping polarized light, scattered light, and fluorescence channels in both two and three dimensions.

Polarized light imaging in the transmission channel during CLSM produced results similar to standard non-laser illumination using a wide-field microscope with cross-polarized filters. Three-dimensional reconstruction from polarized light images was unsuccessful. This is because the transmission channel on the CLSM is not "pin-holed", and out-of-focus polarized light interrupts the image just as it would on a standard system. The significant difference is that CLSM uses z-axis controlled stage and optics, permitting different layers of the sample to be imaged. Though three-dimensional polarized stacks would be out-of-focus, images could possibly be clarified using deconvolution techniques. Deconvolution is the mathematical process of accounting for out-of-focus light without a confocal pinhole, and can even be used to add better definition to 2-D and 3-D CLSM images (McNally et al. 1999). Application of this technique during CLSM imaging could reveal 3-D bone structure in polarized light, enhancing ongoing efforts to relate birefringence in bone to localized strength characteristics (Gebhardt 1905; Ascenzi and Bonucci 1967, 1968; Boyde et al. 1984; Martin et al. 1996; Bromage et al. 2003). Images generated using circularly polarized

light have been linked more directly to bone biomechanical properties than those using cross-polarized light (Boyde et al. 1984; Martin et al. 1996; Bromage et al. 2003). In future efforts, CLSM systems could be optimized for circularly polarized light and simultaneous florescence analysis.

Scattered-light images can also be recorded during polarized-light and fluorescence scanning, but the significance of this phenomenon is not yet clear. Scattered light images and bright points of intensity noted therein are likely related to the "grain" of the material(s) scattering the light. Well-organized, larger particles will scatter light predictably, which is why osteonal lamellae were clearly visible. Smaller, less well-organized particles will scatter much more light however, creating points of detector saturation in the image. Further research may more fully explain the cause for this type of imaging effect and possible applications.

CLSM fluorescence imaging on this system could be accomplished on three separate channels simultaneously, each channel representing light collected at separate and customizable emission wavelengths. Though some degree of emission separation is evident in archaeological fluorescence, for example between "green" and "yellow" channels (Figure 2.7), preliminary investigation shows that, under 458 nm excitation, fluorescent labels in modern and archaeological samples alike emit at a peak of 525 nm with only slight deviation in emission wavelength between given archaeological labels. Regions of the same label have not yet been compared. Taking full advantage of CLSM multichannel fluorescence analysis awaits the development of new techniques in fluorescence histomorphometry. Leading this effort are studies on implant incorporation that add accuracy to tetracycline double labeling techniques (i.e. Takeshita et al. 1997).

The most immediate benefit of two-dimensional CLSM imaging for bone histomorphometry is that it allows the use of samples two or three times thicker than those necessitated by older technology. This decreases sample preparation time. Scratches on the surface can simply be digitally removed rather than labor-intensively sanded and polished. More importantly, thickness artifacts from even thin-sections (~20 µm) can cause error in fluorescence histomorphometric analyses, in comparison with 5 µm sections (Birkenhäger-Frenkel and Birkenhäger 1987). Using CLSM, however, thicker samples can be used without fear of artifacts affecting label intensity or the ease and accuracy of morphological measurement. Despite the fact that a sample may be ~115 µm in thickness, the acquired image is created as if the sample were less than 1 µm deep.

Three-dimensional CLSM also has many advantages; most notably, the generation of a histological cube instead of a cross section or surface area representation. Pioneering work in seriated sectioning has lead to many alterations in ideas regarding the 3-D structure of osteons and compact bone in general (Tapen 1977; Stout et al. 1999; Moshin et al. 2002). A perfect example was Stout and colleagues' observation (1999) that previously described "dumbbell" shaped osteons were actually cross-sectional artifacts single planes of focus cutting through an osteonal branching event. Also notable was Robling and Stout's observations that drifted osteon structure was far more complex than previously assumed (1999). Likewise, questions have been raised as to whether osteon networks could be spiraled. The osteon network, as a whole, may (Cohen and Harris 1958; Hert J et al. 1994; Moshin et al. 2002) or may not (Schumacher S. 1935; Koltze H. 1951; Tapen 1977; Stout et al. 1999) have a slight helical organization relative to the longitudinal axis of long bones. In addition, Cohen and Harris (1958) noted that

individual osteons spiral about their own axes, although it is unclear as to whether they refer to spiral in the osteon's position with reference to an ideal longitudinal axis or actual twist within the structure of the osteon itself.

Results of 3-D CLSM imaging have not yet addressed network-level osteonal organization over large volumes of bone; the total image volume is not great enough currently. As technology and technique in CLSM improve, however, useful information will be provided for Haversian network-level analysis of compact bone. Whereas even high-resolution μCT detects only porous structures, CLSM and other 3-D optical reconstructions include the true paths of osteons by their cement line as well as their canal. In the current research, however, it was found that some osteons demonstrate a perceivable degree of helical organization to *internal* components (lacunae and canaliculi), an effect referred to here as "osteonal twist". Osteonal twist may foster avoidance of microfracture propagation or ensure proper force distribution, especially if trends in clockwise versus counterclockwise orientation bear relation to osteon angle, position within the bone, or ultrastructural collagen and hydroxyapatite orientation in polarized light. In addition, quantitative investigation could provide information on whether all osteons have similar twists or if there is some variation either in degree or direction. In addition, maximum optical penetration should be tested using a variety of optics in order to achieve the best 3-D image depth, while maintaining a useful field of view. Newer laser systems, high numerical aperture/low-power objectives, and even multiphoton techniques could expand the volume of viewable compact bone greatly. Multiphoton laser scanning microscopy has been found to penetrate nervous tissue at depths of around 200 μm (Rodriguez et al. 2003). Preliminary experimentation with

MPLSM at the European Neuroscience Institute, Göttingen, Germany, suggests that either the Biodur@ plastination medium or dry undecalcified bone itself is infrared absorbent enough to cause heat induced separation of the cover slip or even complete laser ablation of bone at higher power objective continuous scanning (Maggiano et al. unpublished data).

These types of anatomical observations provide benefits for all forms of bone histology. Modern investigations of bone microarchitecture could use CLSM technology to bridge the gap between 2-D wide field histomorphometrics and μCT 3-D volumetrics. In physical and forensic anthropology, histological techniques of age estimation, species identification, or disease diagnosis would benefit from multiple sections per sample, but damaging the sample should be kept to a minimum. CLSM allows more efficient use of precious archaeological bone samples, viewing many sections per sample rather than sanding and polishing information away. In general, the 3-D capabilities of CLSM would be enhanced greatly if combined with deconvolution techniques.

Also, of particular archaeological interest is the continued use of CLSM imaging and fluorescence analysis in investigations on ancient fluorescence in archaeological bone. In addition to its use for biomechanical analysis, polarized light has been used as a rough estimate of the preservation state bone at the micro-site level (Schultz 2001). Bone containing bound tetracycline is still active as a bacterial deterrent (Dornbusch 1976; Misra 1991). It could be predicted that fluorescence labels would therefore be more resistant to bacterial diagenesis. Co-localization of positive birefringence in the polarized channel with either the presence or absence of archaeological fluorescence could help determine the differences between *intra vitam* and postmortem tetracycline incorporation.

These are only a few of many research avenues opened by the application of confocal microscopy to bone histology. Capabilities of CLSM imaging far exceed the observational conclusions of the current study and should be quantitatively applied to further efforts in medical, archaeological, and forensic bone sciences. Rejection of out-of-focus light ensures only light from the targeted focal plane is collected. Deeper penetration in imaging means more tissue can be viewed and measured per histological preparation and 3-D microarchitecture is revealed in its true form. CLSM is a more suitable tool for simultaneous fluorescence and polarized light imaging, capable of generating truly serial microscopic sections, providing sufficient detail for observation of cement lines, lamellae, lacunae, and even canaliculi in three dimensions. This is not to say that CLSM replaces older microscopic systems, in fact, it is quite convenient that, in addition to confocal laser scanning, CLSM systems can also be used for standard wide-field transmission, epifluorescence, and polarized light microscopy (in some cases, literally with a flip of the switch). This setup offers the investigator nearly every tool necessary for study of bone histology in one package, a package becoming less and less expensive. Results of the current imaging investigation mark confocal laser scanning microscopy as a preferable optics system for histomorphometric analysis of bone tissue, including archaeological fluorescence investigation.

References

Armelagos GJ. 2000. Take two beers and call me in 1,600 years. Natural History 109(4): 50-4.

Ascenzi A, Bonucci E. 1967. The tensile properties of single osteons. The Anatomical Record 158:160-83.

Ascenzi A, Bonucci E. 1968. The compressive properties of single osteons. The Anatomical Record 161:377-392.

Bassett E, Keith M, Armelagos GJ, Martin D, and Villanueva A. 1980. Tetracycline-labeled human bone from ancient Sudanese Nubia (A.D. 350). Science 209: 1532 -4.

Biggerstaff J, Amirkhosravi A, and Francis JL. 1997. Three-dimensional visualization and quantification of fibrin in solid tumors by confocal laser scanning microscopy. Cytometry 29(2): 122-7.

Biggerstaff J, Amirkhosravi A, and Francis JL. 1998. Three-dimensional quantitation of tumor microvessel density by confocal laser scanning microscopy. Cell Vision. Journal of Analytical Morpholog 4(2): 152-3.

Birkenhäger-Frenkel DH and Birkenhäger. 1987. Bone appositional rate and percentage of doubly and singly labeled surfaces: comparison of data from 5 and 20 μm sections. Bone 8(7): 7-12.

Boyde A, Babayemi J, Jones SJ, and Wolfe LA. 1994. P37 Improved spatial and temporal resolution in tetracycline and calcein labeling in bone and dentine. Bone 15(4): 460.

Boyde A, Bianco P, Portigliatti Barbos M, and Ascenzi A. 1984. Collagen orientation in compact bone: I. A new method for the determination of the proportion of collagen parallel to the plane of compact bone sections. Metabolic Bone Ddiseases and Related Research 5:299-307.

Boyde A and Riggs CM. 1990. The quantitative study of the orientation of collagen in compact bone slices. Bone 11:35-9.

Bromage TG, Goldman HM, McFarlin SC, Warshaw J, Boyde A, and Riggs CM. 2003. Circularly polarized light standards for investigations of collagen fiber orientation in bone. The Anatomical Record 274B:157-68.

Burr DB, Martin RB, Sharkey NA. 1998. Analysis of bone remodeling in skeletal tissue mechanics. New York: Springer-Verlag.

Carr AB, Gerard DA, and Larsen PE. 1996a. The response of bone in primates around unloaded dental implants supporting prostheses with different levels of fit. Journal of Prosthetic Dentistry 76(5): 500-9.

Carr AB, Gerard DA, and Larsen PE. 1996b. Histomorphometric analysis of implant anchorage for 3 types of dental implants following 6 months of healing in baboon jaws. International Journal of Oral Maxillofacial Implants 15(6): 785-79.

Cohen J and Harris WH. 1958. The three-dimensional anatomy of the Haversian system. Journal of American Bone and Joint Surgery 40A: 419-434.

Cook M, Molto E, and Anderson C. 1989. Fluorochrome labelling in Roman period skeletons from Dakhleh Oasis, Egypt. American Journal of Physical Anthropology 80(2): 137-43.

Cooper DML, Turinsky AL, Sensen CW, and Hallgrimsson B. 2003. Quantitative 3D analysis of the canal network in cortical bone by micro-computed tomography. The Anatomical Record 274B: 169-79.

Dornbusch K. 1976. The detection of doxycycline activity in human bone. Scandinavian Journal of Infectious Diseases 9:47-53.

Eriksen EF, Axelrod DW, and Melsen F. 1994. Bone histomorphometry. New York: Raven Press. 1-67.

Frost HM. 1965. Tetracyclines and fetal bones. Henry Ford Hospital Medical Journal 13(4): 403-10.

Frost HM, Villanueva AR, Roth H, and Stanisavljevic S. 1961. Tetracycline bone labeling. The Journal of Clinical Pharmacology 1: 206-16.

Gebhardt W. 1905. Über funktionell wichtige Anordnungsweisen der feineren und gröberen Bauelemente des Wirbeltierknochens. Archiv fuer Entwicklungsmechanik der Organismen 20:187-322.

Hert J, Fiala P, and Petryl. 1994. Osteon orientation of the diaphysis of the long bones in man. Bone 15(3): 267-77.

Hoerman KC. 1975. Spectral characteristics of tetracycline-induced luminescence in rat teeth and bones. Journal of Dental Research 54: 131-6.

Hope C A. 2001. Observations on the dating of the occupation at Ismant el-Kharab. In: Marlow CA and Mills AJ, editors. The Oasis Papers 1: The Proceedings of the First Conference of the Dakhleh Oasis Project. Oxbow Books: Oxford. 43–59.

Horvath JJ and Glazier SA. 1993. Fluorescence measurements of tetracycline in high cell mass for fermentation monitoring. American Biotechnology Laboratory 11(7): 44.

Jaworski ZFJ. 1992. Haversian systems and Havarsian bone. In: Hall BK, editors. Bone metabolism and mineralization Vol. 4. Boca Raton, CRC Press. 21-45.

Jouk PS, Usson Y, Michalowicz G, Parazza F. 1995 Mapping the orientation of myocardial cells by means of polarized light and confocal scanning laser microscopy. Microscopy Research and Technique 30:480-90.

Keith M and Armelagos GJ. 1983. Naturally occurring antibiotics and human health. in: Romanuuci L, Moerman D, and Tancredi L, editors. The Anthropology of Medicine. New York: Bergin and Garvey Publishers.

Keith M and Armelagos GJ. 1988. An example of in vivo tetracycline labeling: Reply to Piepenbrink. Journal of Archaeological Science 15: 595-601.

Koltze H. 1951. Studie zur ausseren form der osteone. Zeitschrift Fuer Anatomie und Entwicklungsgeschichte 115:584–91.

Maggiano C, Dupras T, and Biggerstaff J. 2003. Ancient antibiotics: evidence for tetracycline in human and animal bone from kellis. In: AJ Mills and CA Hope, editors. The Dakhleh Oasis Monograph Vol. 3. Oxford: Oxbow Books. 331-44.

Martin RB and Burr DB. 1989. Structure, function, and adaptation of compact bone. New York: Raven Press.

Martin RB, Lau ST, Mathews PV, Gibson VA, and Stover SM. 1996. Collagen fiber organization is related to mechanical properties and remodeling in equine bone: a comparison of two methods. Journal of Biomechanics 29(12):1515-1521.

McNally JG, Karpova T, Cooper J, Conchello JA. 1999. Three-dimensional imaging by deconvolution microscopy. Methods 19;373-85.

Milch RA, Rall DP, and Tobie JE. 1957. Bone localization of tetracyclines. Journal of the National Cancer Institute 19(1): 87-93.

Milch RA, Rall DP, and Tobie JE. 1958. Fluorescence of tetracycline antibiotics in bone. The Journal of Bone and Joint Surgery 40(4); 897-910.

Misra DN. 1991. Adsorption and orientation of tetracycline on hydroxyapatite. Calcified Tissue International 48(5), 362-7.

Mohsin S, Taylor D, and Lee TC. 2002. Three-dimensional reconstruction of Haversian systems in ovine compact bone. European Journal of Morphology 40(5): 309-315.

Molto JE, 2001. The comparative skeletal biology and palaeoepidemiology of the people from Ein Tirghi and Kellis, Dakhleh Oasis, Egypt. In: Marlow CA and Mills AJ, editors: The Oasis Papers 1: The Proceedings of the First Conference of the Dakhleh Oasis Project. Oxbow Books: Oxford. 81–100.

Piepenbrink H, Herrmann B, and Hoffman P. 1983. Tetracylintypische fluoreszenzen and bodengelagerten skeletteilen. Zeitschrift fur Rechtsmedizin 91: 71-4.

Richman EA, Ortner DJ, Schulter-Ellis FP. 1979. Differences in intracortical bone remodeling in three aboriginal American populations: possible dietary factors. Calcified Tssue International 28:209-214.

Robling AG and Stout SD. 1999. Morphology of the drifting osteon. Cells Tissues Organs 164: 192-204.

Rodriguez A, Ehlenberger D, Kelliher K, Einstein M, Henderson SC, Morrison JH, Hof PR, Wearne SL. 2003. Automated reconstruction of three-dimensional neuronal morphology from laser scanning microscopy images. Methods 30:94-105.

Rush T, Pirok D, and Frost HM. 1966. Fractional labeling: the fraction of actively forming osteons that take tetracycline labels in normal human bone. Henry Ford Hospital Medical Bulletin 14: 255-63.

Schultz M. 1988. Methoden der Licht und Elektronenmikroskopie. In: Knußmann R, editor. Anthropologie: Handbuch der vergleichenden Biologie des Menschen. Stuttgart: Fischer Verlag 1(1): 698–730.

Schultz M 2001. Paleohistopathology of bone: a new approach to the study of ancient diseases. Yearbook of Physical Anthropology 44: 106–47.

Schumacher S. 1935. Zur Anordnung der gefässkanäle in der diaphyse langer röhrerknochen des menschen. Zeitschrift Fuer Zellforschung und Mikroskopische Anatomie Abteilung Histochemie 38:145–160.

Stout SD, Brunsden BS, Hildebolt CF, Commean PK, Smith KE, Tappen NC. 1999. Computer-assisted 3D reconstruction of serial sections of cortical bone to determine the 3D structure of osteons. Calcified Tissue International 65: 280-84.

Takeshita F, Iyama S, Aykawa Y, Akedo H, and Suetsugu T. 1997. Study of bone formation around dense hydroxyapatite implants using light microscopy, image processing and confocal laser scanning microscopy. Biomaterials 18:317-322.

Tappen NC. 1977. Three-dimensional studies of resorption spaces and developing osteons. American Journal of Anatomy 149: 301-331.

Taylor T and Frost HM. 1966. The existence of a zone of finite thickness during tetracycline labeling of bone. Henry Ford Hospital Medical Bulletin 14: 255-63.

Villanueva AR, Kujawa M, Mathews CHE, and Parfitt AM. 1983. Identification of the mineralization front: comparison of a modified toluidine blue stain with tetracycline fluorescence. Metabolic Bone Diseases and Related Research 5: 41-5.

Wachter NJ, Augat P, Krischak GD, Mentzel M, Kinzl L, and Claes L. 2001. Prediction of cortical bone porosity in vitro by microcomputed tomography. Calcified Tissues International 68:38-42.

Wachter NJ, Augat P, Krischak GD, Mentzel M, Sarkar MR, Ebinger T, Kinzl L, Claes L, and Augat P. 2002. Correlation of bone mineral density with strength and microstructural parameters of cortical bone in vitro. Bone 31(1). 90-5.

CHAPTER 4

GENERAL DISCUSSION

The results of these studies support the use of confocal laser scanning microscopy for continued research on tetracycline labels in modern and ancient bone and encourage the use of this technique for histological imaging of dry undecalcified archaeological bone material. Overflowing the boundaries of archaeological bone investigation, the combined advantages of simultaneous spectral analysis and improved two- and three-dimensional fluorescence imaging, polarized light, and scattered light imaging, encourage extensive application of CLSM in anthropological, medical, and forensic bone investigation.

During anthropological examination, when bone material is too precious for destruction, CLSM could be used to take an optical longitudinal section of the bone surface (~100 um thick), with no damage to the bone what so ever. This could be very useful for the study of lesions in paleopathology for example since it seems clear that TC fluorescence (whether pre- or postmortem) should be bright enough to generate a clear image. It would be interesting to compare this application of CLSM with currently improving high-resolution μCT scanning. In medical research, μCT is able to resolve large volumes of bone microstructure to the level of the Haversian canal but cannot yet image cement lines, lacunae, or canaliculi or determine the difference between old and newly formed bone (Wachter et al. 2001; Wachter et al. 2002; Cooper et al. 2003). CLSM has the capability to do all this and simultaneously provide spectral, polarized

light, and scattered light data. Its only limitation is that so far the volume of bone microstructure reconstructed is rather small. Techniques developed in the future could increase the volume of bone that can be imaged using CLSM, piecing together multiple z-stacks to follow one or several osteons for greater depths. This would have very interesting benefits for fluorochrome labeling techniques used in histomorphometry for fracture healing, osteoporosis, or surgical implant incorporation studies. For application to forensics CLSM could be used to provide data on unexplored variables of bone microstructure for identification of skeletal remains or even contribute information on time since death via fluorescence identification of via microbe succession in decomposing bone material, as this has been achieved for other purposes in complex biofilm assays (Packeroff et al. 2002).

Future exploration of these ideas requires a high level of multidisciplinary cooperation. Especially in their more derived forms, confocal microscopy and multiphoton microscopy systems are still very expensive. Collaboration is the key to not only to the successful procurement of the technology itself but for its correct application and interpretation. These factors in mind, CLSM systems are marked as a worthy center post for future experimentation involving cooperative efforts in anthropology, medicine, and forensics.

References

Cooper DML, Turinsky AL, Sensen CW, and Hallgrimsson B. 2003. Quantitative 3D analysis of the canal network in cortical bone by micro-computed tomography. The Anatomical Record 274B:169-79.

Packeroff G, Lawrence JR, and Thomas R. 2002. In Situ Confocal Laser Scanning Microscopy of Protozoans in Cultures and Complex Biofilm Communities. Acta Protozoology 41:245-253.

Wachter NJ, Augat P, Krischak GD, Mentzel M, Kinzl L, and Claes L. 2001. Prediction of cortical bone porosity in vitro by microcomputed tomography. Calcified Tissues International 68:38-42.

Wachter NJ, Augat P, Krischak GD, Mentzel M, Sarkar MR, Ebinger T, Kinzl L, Claes L, and Augat P. 2002. Correlation of bone mineral density with strength and microstructural parameters of cortical bone in vitro. Bone 31(1). 90-5.